1959

Circumferential distortion of the inlet flow in an axial compressor.

Shinbaum, Marvin S.

Massachusetts Institute of Technology

CIRCUMFERENTIAL DISTORTION OF THE INLET FLOW IN AN AXIAL COMPRESSOR

MARVIN S. SHINBAUM

CIRCUMFERENTIAL DISTORTION OF THE INLET FLOW IN AN AXIAL COMPRESSOR

BY

CAPT. MARVIN S. SHINBAUM, U.S.M.C.

B.A. , SOUTHWESTERN AT MEMPHIS
(1950)
B.S.A.E. , UNITED STATES NAVAL POSTGRADUATE SCHOOL
(1958)

SUBMITTED IN PARTIAL FULFILLMENT OF THE
REQUIREMENTS FOR THE DEGREE OF
MASTER OF SCIENCE IN
AERONAUTICAL ENGINEERING

at the

MASSACHUSETTS INSTITUTE OF
TECHNOLOGY
May 1959

CIRCUMFERENTIAL DISTORTION OF THE INLET FLOW IN AN AXIAL COMPRESSOR

by

MARVIN S. SHINBAUM

Submitted to the Department of Aeronautics and Astronautics on May 25, 1959, in partial fulfillment of the requirements for the degree of Master of Science in Aeronautical Engineering.

ABSTRACT

An investigation has been made of the effect of the isolated blade row in a single-rotor, axial flow compressor upon a circumferentially distorted inlet velocity profile. Flow rate and chord/pitch ratio were varied to determine the influence of these parameters on the velocity defect. Experimental results were compared with two theories, both based on a two-dimensional, incompressible, inviscid actuator disc analysis. It was found that both theories underestimate the experimentally observed attenuation due to the rotor, however, the more recent analysis by Seidel gives better agreement than that of Rannie and Marble. Seidel's theory correctly predicts more attenuation with an increase in chord/pitch ratio. The gain in attenuation due to reduced flow rate was not accurately predicted by either theory, but again Seidel's prediction is closer to experiment.

Thesis Supervisor: Yasutoshi Senoo

Title: Assistant Professor of Mechanical Engineering

Cambridge, Massachusetts
May 25, 1959

Professor Alvin Sloane
Secretary of the Faculty
Massachusetts Institute of Technology
Cambridge 39, Massachusetts

Dear Professor Sloane:

In accordance with the regulations of the faculty, a thesis entitled Circumferential Distortion of the Inlet Flow in an Axial Compressor is hereby submitted in partial fulfillment of the requirements for the degree of Master of Science in Aeronautical Engineering.

Respectfully,

Marvin S. Shinbaum

Marvin S. Shinbaum

ACKNOWLEDGEMENTS

The author gratefully acknowledges the assistance and counsel of Professor Yasutoshi Senoo in his capacity as thesis supervisor, and owes particular gratitude to Mr. Barry S. Seidel for his patient, careful and competent guidance as project leader. Professor E. S. Taylor participated in discussions of this thesis, and provided continuous encouragement.

The experiments herein described were conducted under the sponsorship of the General Electric Company, the Westinghouse Electric Corporation, and the Allison Division of General Motors Corporation.

Probe construction and equipment fabrication were the work of Mr. Basil Kean and Mr. Paul Wassmouth respectively. Final typing was done by Natalie Appleton.

The author was assigned to the U. S. Naval Administrative Unit at the Massachusetts Institute of Technology while completing the graduate work of which this thesis is a part.

TABLE OF CONTENTS

LIST OF FIGURES

SYMBOLS

b	1/2 blade chord
C_D	$C_D(\tan\beta_1)$; Seidel loss coefficient
C_D'	$dC_D/d\tan\beta_1$
F	blade force
H	$p/\rho + Uu + Vv$
i	incidence angle
n	number of distortion screens
P	average pressure
P	$P(\tan\beta_1)$; Rannie-Marble loss coefficient
P'	$dP/d\tan\beta_1$
$\wp$	p/ρ
p	stream static pressure
p	disturbance pressure
r	geometric mean radius of flow annulus
Re_{2b}	Reynolds number based on blade chord
S	blade interval; pitch
U	mean axial component of velocity
u	axial component of disturbance velocity
V	mean tangential component of velocity
V_r	Ωr; rotor velocity at geometric mean radius
v	tangential component of disturbance velocity
w_o	mean relative velocity
x	axial distance
Y	non-dimensional circumferential reference position $(y/\frac{2\pi r}{n})$
y	distance in circumferential direction

β	relative flow angle
η	auxiliary variable
Θ	Uv - Vu
θ	absolute flow angle
ρ	air density
Ω	rotational speed of rotor

Subscripts

m	mean value
r	rotor
o	stagnation condition
1	immediately upstream of rotor (0-, y)
2	immediately downstream of rotor (0+, y)
$\pm\infty$	far downstream or upstream from the rotor

Superscript

*	complementary function

CIRCUMFERENTIAL DISTORTION OF THE INLET FLOW IN AN AXIAL COMPRESSOR

1. INTRODUCTION

Since modern, high-performance aircraft must operate over a wide range of flight conditions, the gas-turbine power plants for such aircraft must evolve from designs which attempt to provide satisfactory engine performance over a comparable range of inlet velocity distributions. Inlet velocity distortions in axial flow power plants may be produced by separation at the inlet lip when operating at high angles of attack or off-design conditions, or by separation from the walls when the flow is turned or diffused too rapidly within the inlet duct. Non-uniformity of the inlet velocity presentation may be expected to result in reduction in compressor stall margin, and non-uniform, thus inefficient compression of the working fluid.

While jet engines differ in their acceptance of inlet flow distortions, both theory and investigations of representative compressor inlet stages indicate that velocity distortion will be reduced across a rotor because that portion of a distorted flow having an energy level lower than some mean value is energized more than portions having an energy level higher than the mean. Further investigation of the problem of inlet flow distortion in axial turbo-machines is justified in order to formulate design criteria for compressors which will accept more severe distortions, and for ducting which will reduce distortions before reaching the compressor.

Circumferential distortions of the inlet flow, which appear to cause the most significant reduction in compressor stall margin, have been the subject of only a few analytical publications. Notable among these are the work of Ehrich (Reference 1), and that of Rannie and Marble (Reference 2). In both of these investigations, a quasi-steady actuator disc analysis was applied to an incompressible, inviscid flow in an axial turbomachine with hub/tip ratio close to unity, allowing the problem to be treated two-dimensionally.

Seidel (Reference 3), in a more recent investigation, has compared the theories of Ehrich and Rannie-Marble and concluded that they are the same for the case of an isolated blade row. He suggests an improvement to the previous theory in which a more general, unsteady actuator disc analysis is used. The assumption from previous theory of constant leaving angle relative to the rotor is relaxed in favor of the Kutta condition, and the introduction of unsteady blade forces permits investigation of the effect of variations in chord/pitch ratio.

The experimental investigation herein described served to compare the two existing theories with the performance of a single-rotor, axial flow compressor. A single inlet screen configuration was used for all tests, and data were obtained for four flow rates at each of two values of chord/pitch ratio. In all cases, measurements were taken at four axial locations:

i) $(-\infty)$ - far upstream of the rotor

ii) (1) - immediately upstream of the rotor

iii) (2) - immediately downstream of the rotor

iv) $(+\infty)$ - far downstream of the rotor

Comparison with theory is presented for the maximum and minimum flow rates for each of the two chord/pitch ratios.

2. APPARATUS AND INSTRUMENTATION

2.1 Compressor

Figure 1 is a section view of the compressor used in these tests. The isolated rotor and a portion of the instrumentation arrangement are shown in Figure 2. Essential rotor dimensions were:

Outside diameter	23.25 inches
Hub/tip ratio	0.75
Blade chord	1.50 inches
Blade aspect ratio	2.84
Blade tip clearance	0.035 inces

The blade sections were NACA 65-(12)10 airfoils with a stagger at the mean radius of 52.7 degrees measured from the axial direction. The blades were twisted linearly 9.70 degrees from root to tip. A rotor speed of 1000 rpm was used in the tests for which results are presented. Inlet air was introduced radially through damping screens.

2.2 Distortion Screens

The choice of an inlet distortion screen arrangement was dictated by the desire to reduce the solidity at the edges of a screen segment, thus avoiding inlet distortion profiles complicated by the formation of concentrated vortices in these regions. When such vortices do occur, a velocity distribution similar to that in Figure 3 would be anticipated from potential theory, and such velocity distributions are reported in the experimental results of Reference 4.

The most desirable inlet screen arrangement provides a velocity profile which is readily defined mathematically and/or typical of distortion in actual machinery, e.g. a square-wave or sinusoidal inlet disturbance. While relatively simple to represent mathematically, the sine wave is difficult to obtain experimentally, leading to the choice of a square wave profile generator. For generation of a square-wave profile, the ideal solidity distribution in the circumferential direction is shown in Figure 4, however such screening is not readily available.

Several combinations of square-mesh screens of different solidity were tested to obtain a profile which approximated a square wave, despite the appearance of moderate, vortex-induced peaks. The final arrangement consisted of a 45 degree screen of mesh 4 x 4, wire size 23 (A.W.G.), on which was superimposed symmetrically a 36 degree screen of mesh 6 x 6 made from number 25 wire. Three of the larger screens provided the rigidity for an annular frame which is shown in Figure 5. In order to achieve relative motion between screen and probes, the system of screens and frame was positioned stepwise through a complete cycle of 120 degrees by means of a reel and cord arrangement (Figure 6) which permitted readings every 1.42 degrees of arc. The use of three distortion screen segments and the location of the probes far upstream and far downstream of the rotor were dictated by considerations outlined in Appendix A.

2.3 Probes

Shown in Figure 7 is a three-hole Fecheimer tube of the type described in Reference 5 which was used to measure yaw angle, static pressure and total pressure. This probe has three 0.012 inch holes drilled

into a 0.125 inch stock tube at a distance of 0.25 inches from a hemispherical tip. The drillings, which are spaced at 42 degrees of arc, connect with three hypodermic tubes contained inside the stock tube. The center hole points into the flow when the pressures at the two outer drillings are equalized.

The yawing of the probes and the measurement of pressure at the four stations shown in Figure 8 were accomplished through the use of a pressure switching circuit and a pair of strain gage pressure transducers connected to a D-C calibrating device. This transducer equipment, which incorporates a transistorized D-C amplifier, was manufactured by the Dynamic Instrument Company of Cambridge, Massachusetts.

Yaw angles were measured directly with protractors mounted on the compressor shell. Initial alignment of the probes involved removal of the distortion screens to assure axial flow at the upstream stations. Then each probe in turn was placed in the farthest upstream station, yawed until the center hole was aligned with the flow, and the indicator arm set to read 90 degrees on the protractor.

Volume flow of air through the compressor was controlled by the position of a damper valve shown in Figure 1, and the rpm of the rotor. A counter mounted on the compressor control panel measured damper setting, while an electrical strobotac indicated the rotor speed.

3. EXPERIMENTAL PROCEDURE

The highest flow rate for each value of chord/pitch ratio was fixed by the maximum damper opening and the minimum flow rate determined by the onset of rotating stall. In determining the lower limit of damper setting it was observed that rotating stall occurred over a range of damper settings depending on such factors as local disturbances at the inlet bell-mouth and random noise. As a consequence, early attempts to operate too close to this critical range resulted in runs which were only partially completed when rotating stall occurred. A low flow setting was finally chosen which permitted continuous readings, and two intermediate damper settings between the high and low flow rates were selected for investigation. Significant parameters for the maximum and minimum flow rates at each value of chord/pitch ratio are listed in Table 3 - I.

TABLE 3-I

Flow Parameters

Chord/Pitch	1.05		0.525	
$U/\Omega r$	.567	.460	.514	.391
$U_{-\infty}$ (ft/sec)	53.6	41.2	50.6	36.8
U_1 (ft/sec)	49.5	40.6	46.2	36.0
U_2 (ft/sec)	51.7	43.4	50.5	39.9
$U_{+\infty}$ (ft/sec)	50.4	41.3	46.1	35.0
i_m (°)	9.3	15.3	8.8	16.1
w_o (ft/sec)	91.2	82.6	90.6	81.8
Re_{2b}	40,500	32,100	36,500	27,400

For the maximum value of chord/pitch ratio ($2b/s = 1.05$), 44 blades were mounted on the rotor which was operated at 1,000 rpm throughout. The resulting low air velocity ($U \cong 50$ ft/sec) permitted the flow to be treated as incompressible.

To reduce the chord/pitch ratio by one-half, 22 blades were removed alternately, and the resulting holes in the rotor rim filled by aluminum hexagonal-head bolts. Again, for the maximum and minimum flow rates, the rotor was operated at 1,000 rpm, but, in order to duplicate the intermediate flow rates of the higher solidity case, it was necessary to adjust the damper settings slightly and operate at 1,050 rpm. An increase in the stall-free operating range due to removal of half the blades permitted low flow rate measurements at a reduced damper setting.

For each flow rate, measurements of flow angle, static and stagnation pressure were recorded approximately every 7.10 degrees of screen rotation except in regions near the edges of the distortion screen. Here readings every 1.42 degrees were required to define the profile more accurately. The decision to rotate the screen rather than the probes was based on:

i) the knowledge from previous experiments with the same compressor that the flow without distortion screens was axisymmetric;

ii) the relative simplicity of the screen rotation mechanism required (Figure 6) in comparison with the extensive modification necessary in order to rotate the the four probes through a complete cycle of 120 degrees.

Measurements were taken at the mean geometric radius of the flow annulus

to avoid boundary layer effects and thus achieve a maximum degree of two-dimensionality.

Prior to each run, ambient pressure and temperature were recorded from a standard mercury barometer and Fahrenheit thermometer respectively. Also recorded were the zero (atmospheric) readings of the two pressure transducers in terms of a resistance bridge balancing current. The compressor was then brought up to speed and the damper set. For each data point, each probe in turn was yawed until equalized pressures at the outer taps produced a null (balanced) reading on the indicating dial, and the flow angle was recorded. The stagnation pressure (center hole) and the indicated pressure p_i at one of the outer holes were then measured by comparison with atmospheric pressure. In subsequent calculations these readings were related to the free stream static pressure by means of an experimentally determined probe calibration constant $k = \frac{p - p_i}{p - p_o}$; the values of p_o and p were then used to compute velocity from $V = \sqrt{\frac{2}{\rho}}\sqrt{p_o - p}$. Density was calculated from the perfect gas relation making use of ambient pressure and temperature. No correction was made for stagnation pressure gradient since previous experimental measurements indicated that this effect was negligible.

4. ANALYSIS OF RESULTS

4.1 Method of Presentation

It was convenient to plot the experimental results in terms of the quantities

$$H = p/\rho + Uu + Vv$$

$$\Theta = Uv - Vu$$

$$\mathcal{P} = p/\rho$$

for ready comparison with theory. U and V were determined from graphical integration of plots of local velocity components, and the perturbation velocities u and v from the difference of the mean values and the local components. Perturbation pressures (p) were calculated in a similar manner.

Experimentally determined values of H_2/U^2, Θ_1/U^2, Θ_2/U^2, $\mathcal{P}_1/U^2$ and $\mathcal{P}_2/U^2$ are presented coincidentally with curves of the same quantities obtained from the theories of Seidel and Rannie-Marble in Figures 9-1 through 9-4. No presentation of results is given for the intermediate flow rates since the effect of flow rate is most clearly demonstrated by comparison of the highest and lowest values obtainable.

4.2 Comparison with Theory

A brief development of the two methods of analysis used for the theoretical results is given in Appendix B where the notation of Rannie and Marble has been modified in the case of Θ and $\mathcal{P}$ to agree with that of Seidel. Input data for both theories was obtained from 51 equi-spaced points on the curves of H_1/U^2 shown in Figures 9.

Although both theories underestimated the attenuation of the velocity distortion due to the rotor, it is apparent that the Seidel theory gives consistently better agreement for the downstream predicted quantities H_2, Θ_2, and P_2. The Rannie and Marble analysis gives a more accurate prediction of the upstream values Θ_1 and P_1. Agreement in either case may be limited by the assumption of inviscid flow and by the difficulty involved in locating ± 0 accurately. No real flow is entirely without viscosity, and, since the Cauchy-Riemann functions Θ and P vary as $\exp\left(-\frac{nx}{r}\right)$, an error of 1.5 inches (the distance from the blade row midplane to the nearest probes, Figure 8) in the location of the upstream or downstream zero point means a reduction in these quantities to $\exp\left(-\frac{3 \times 1.5}{10.62}\right) = .64$ of their value at the actuator disc.

The quantity H_2/U^2 was chosen as a suitable parameter for determining the degree of attenuation of the velocity distortion since this quantity is the perturbation velocity within a constant. That is, $H_2/U^2 = H_{+\infty} / U^2 = \frac{u_{+\infty}}{U} (1 + V_2^2/U^2)$. The effect of flow rate on attenuation is shown in Figure 10, and the effect due to solidity in Figure 11. The Seidel theory is seen to correctly predict increased attenuation for a higher value of chord/pitch ratio. Since the Rannie-Marble analysis assumes constant chord/pitch ratio, no comparison is possible for that theory. While neither theory accurately predicts the experimentally observed gain in attenuation with a reduction in flow rate, Seidel's theory shows improved agreement with experiment over that of Rannie and Marble.

It was concluded that, in general, the Seidel theory gives a better prediction of the performance of a single-rotor axial compressor with circumferentially distorted inlet velocity profile.

4.3 Applicability to Theory

To test the applicability of the experimental results to the theories considered, three assumptions common to both analyses were examined. The continuity condition assumes $U_{-\infty} = U_1 = U_2 = U_{+\infty}$; experimental results (Table 3-I) reveal a consistent variation of 6 to 9 per cent between the highest and lowest value, with high readings occurring at stations $-\infty$ and 2, low readings at 1 and $+\infty$. This variation may be the result of a change in radial distribution of velocity with axial location, but is probably due to the influence of turbulence in the wake of the screen and rotor. Appendix C is a discussion of the influence of turbulence on pressure measurements. The influence of turbulence was presumed least at $+\infty$, and this value of U was used as the representative velocity for each flow rate.

Theory assumes that $H(-\infty, y) = H_1(0-, y)$ and $H_2(0+, y) = H(+\infty, y)$; Figure 12 indicates that H_{+0}/U^2 decays before reaching the downstream measuring station, probably due to viscous effects. The upstream curves agreed more closely, but no conclusion could be drawn from their comparison.

Finally, the linearized forms of the equations of motion and continuity are predicated on small perturbations. If the quantity $\frac{u-\infty}{U}$ is used as a measure of perturbation intensity, the third term in the expansion $(1+u/U)^2 = 1+2u/U + (u/U)^2$ is neglected in linear theory. Since the maximum value of $\frac{u-\infty}{U}$ observed experimentally was .35, the highest value of the neglected term in comparison with the term retained is $\frac{(.35)^2}{2(.35)} = .175$.

It was concluded that experimental conditions sufficiently

approximated the three assumed conditions to make the tests valid. The degree of validity would be imporved with correction factors based on additional knowledge of the magnitude of effects due to turbulence and viscosity.

5. CONCLUSION

An experimental investigation of a single-rotor axial flow compressor has determined the effect of the isolated blade row on a forced circumferential distortion in the inlet velocity profile. For the distortion-screen configuration tested, it was shown that the velocity defect was attenuated by passage through the moving blade row, and that the degree of attenuation increased with reduced flow rate or increased chord/pitch ratio.

Experimental results were compared with two theories, both based on a two-dimensional, incompressible, inviscid actuator disc analysis. It was found that both theories underestimate the attenuation due to the rotor, although the theory of Seidel gives better agreement with experiment than that of Rannie and Marble. Seidel's theory correctly predicts an increase in attenuation for increased chord/pitch ratio. Neither theory accurately predicts the experimentally observed gain in attenuation with reduced flow rate, however agreement is improved with the Seidel theory. It was generally concluded that the Seidel theory gives a more accurate prediction of isolated rotor performance with regard to a circumferentially distorted inlet velocity distribution.

Comparison was made between experimental results and three limiting assumptions common to both analyses, namely, continuity, constant $H(x,y)$

upstream or downstream of the rotor, and small perturbations. It was concluded that the experiments were applicable to the theories considered.

Further investigation of distorted inlet flows in axial compressors might provide information on:

i) radial velocity distribution in a circumferentially distorted flow field;

ii) the effect of multiple blade rows including stators, rotors, and inlet guide vanes;

iii) the magnitude of viscous and turbulence effects;

iv) an easily-applied relationship between attenuation and mean flow (for design purposes).

BIBLIOGRAPHY

1. Ehrich, F. F., "Circumferential Inlet Distortions in Axial Flow Turbomachinery", Journal of the Aeronautical Sciences, June 1957.

2. Rannie, W. D. and Marble, F. E., "Unsteady Flows in Axial Turbomachines", Guggenheim Jet Propulsion Center, C.I.T. Publication No. 94.

3. Seidel, B. S., "Asymmetric Inlet Flow in Axial Turbomachines", M.I.T. Sc.D. Thesis in Mechanical Engineering, May 1959.

4. Carter, F. R., "Circumferential Inlet Distortion in an Axial Flow Compressor", M.I.T. S.M. Thesis in Aeronautical Engineering, May 1958.

5. Horlock, J. H., "Instrumentation used in Measurement of the Three-Dimensional Flow in an Axial Flow Compressor", Aeronautical Research Council Current Paper No. 321, London, March 1955.

6. Seidel, B. S., "A Boundary Relationship between Two Cauchy-Riemann Variables", M.I.T. Gas Turbine Laboratory Technical Memorandum 34-A, 1958.

7. Dean, R. C., "Aerodynamic Measurements", M.I.T. Gas Turbine Laboratory Publication, 1953.

8. Schubauer, G. B., Spangenberg, W. G. and Klebanoff, P. S., "Aerodynamic Characteristics of Damping Screens", NACA Technical Note 2001, 1950.

APPENDIX A

Criterion for Inlet Distortion Wavelength and Axial Location of Probes

In the analysis of Reference 1 it was concluded that any circumferential distortion of width $\frac{2\pi r}{n}$ will induce local disturbances at the rotor. However, these disturbances will diminish exponentially upstream and downstream of the rotor, the decay factor being $\exp\left(\frac{-n|x|}{r}\right)$.

Since three sections of distortion screen (Figure 5) were used in these tests, the distortion width was $\frac{2\pi r}{n} = 6.67\pi$ inches and $\frac{r}{n} = 3.34$ inches. For the probes located 22.0 inches upstream and downstream from the plane of the rotor, the rotor influence was reduced by

$$\exp\left(\frac{-22.0}{3.34}\right) = 0.001.$$

APPENDIX B

Methods of Analysis

In the following discussion, that portion of Reference 2 dealing with a circumferential inlet distortion approaching an isolated rotor has been extracted (with notational modification) to indicate the assumptions of the Rannie and Marble solution and the procedure for calculation of the corresponding theoretical curves of Figure 9.

No exposition is given of the Seidel solution, however, the differences in assumptions are emphasized, and the sequence of development outlined briefly.

B1 Theory of Rannie and Marble

In the description of the disturbance flow field, let x and y be rectangular coordinates with the axis of y parallel to the plane of the cascade, Figure 13. The average velocity components and pressure are U, V and P, all constant upstream and downstream of an isolated blade row. The disturbance velocity components and pressure are u, v and p, all with average values zero. The disturbance is assumed periodic in the y-direction, and of wave length sufficiently large, compared with the blade gap, that the distortions produced by individual blades on the disturbance pattern are ignored.

For small disturbances the equations of motion and of continuity in linearized form are:

$$U \frac{\partial u}{\partial x} + V \frac{\partial u}{\partial y} = - \frac{1}{\rho} \frac{\partial p}{\partial x} \qquad (1a)$$

$$U \frac{\partial v}{\partial x} + V \frac{\partial v}{\partial y} = - \frac{1}{\rho} \frac{\partial p}{\partial y} \tag{1b}$$

$$\frac{\partial u}{\partial x} + \frac{\partial v}{\partial y} = 0 \tag{1c}$$

Completely equivalent, but more illuminating are the following three equations:

$$\left[U \frac{\partial}{\partial x} + V \frac{\partial}{\partial y} \right] \left[\frac{p}{\rho} + Uu + Vv \right] = 0 \tag{2}$$

$$\frac{\partial}{\partial y} \left[Uv - Vu \right] = \frac{\partial}{\partial x} \left(\frac{p}{\rho} \right) \tag{3}$$

$$\frac{\partial}{\partial x} \left[Uv - Vu \right] = - \frac{\partial}{\partial y} \left(\frac{p}{\rho} \right) \tag{4}$$

The first of these is the condition that the perturbation of total pressure is constant along the mean stream lines. The second two equations show that the combination $[Uv - Vu]$ (proportional to flow angle perturbation) and the static pressure divided by density are potential functions and satisfy the Cauchy-Riemann conditions. For convenience in the analysis, the following definitions are introduced:

$$\boxminus \equiv \frac{p}{\rho} + Uu + Vv \tag{5}$$

$$\ominus \equiv Uv - Vu \tag{6}$$

$$\wp \equiv \frac{p}{\rho} \tag{7}$$

The following relations then hold,

$$H(x,y) = H\left(0, y - \frac{V}{U}x\right) \tag{8}$$

$$\frac{\partial \Theta}{\partial y} = \frac{\partial \mathcal{P}}{\partial x} \; ; \quad \frac{\partial \Theta}{\partial x} = -\frac{\partial \mathcal{P}}{\partial y} \tag{9}$$

and two functions are sufficient to define the disturbance flow completely.

For a semi-infinite flow field upstream or downstream of a blade row, the functions can be given in simple terms. Θ and $\mathcal{P}$ approach zero far from the cascade and if the blade row is at x = 0, then for $\Theta(0,y)$ given, $\mathcal{P}(0,y)$ can be found from

$$\left.\begin{aligned} \mathcal{P}(0+,y) &= \int_0^1 \Theta(0+,\eta)\cot\pi(y-\eta)\,d\eta \equiv \Theta^*(0+,y) \\ \mathcal{P}(0-,y) &= -\int_0^1 \Theta(0-,\eta)\cot\pi(y-\eta)\,d\eta \equiv \Theta^*(0-,y) \end{aligned}\right\} \tag{10}$$

Reference 6 contains a developemnt of this relationship between complementary functions.

Conversely, $\Theta(0+, y) = -\mathcal{P}^*(0+, y)$ and $\Theta(0-, y) = \mathcal{P}^*(0-, y)$ where the wave length is unity. Θ and $\mathcal{P}$ may be found for all values of x and y if $\Theta(0, y)$ or $\mathcal{P}(0, y)$ is given. Hence the disturbance flow is described completely by H(0, y) and $\Theta(0, y)$ or $\mathcal{P}(0, y)$.

If the flow is assumed locally quasi-steady, three conditions relating to conservation of mass, momentum and energy can be prescribed to give the local outlet flow in terms of the local inlet flow. Let U_1, V_1, P_1 and U_2, V_2, P_2 be the average velocity components and pressures upstream and downstream of a rotor. Let u_1, v_1, p_1 and u_2, v_2, p_2 be the perturbation values at (0-, y) and (0+, y) respectively. Then the matching

conditions at the blade row are those listed in Table B-I where, for the equations in H, Θ and P, the following values are specified in any experiment:

$$A_r = \frac{V_r - V_1}{U} + P_r'$$

$$B_r = -\frac{(V_r - V_1)^2 - (V_r - V_2)^2}{U V_r} + \frac{V_r - V_1}{U} + \frac{2U}{V_r} P_r - P_r'$$

$$\alpha_r = \frac{V_1}{U} \quad ; \quad \beta_r = -\frac{U^2 + V_1^2}{U V_r}$$

$$\gamma_r = -\frac{U^2 + V_2^2 - (V_r)(V_2)}{U V_r}$$

The symbol P_r represents a blade loss coefficient which is a prescribed function of $\tan\beta_1$. P_r' is the slope of the P_r $(\tan\beta_1)$ curve at a point.

TABLE B-I

Boundary Conditions for Rannie-Marble

Matching Condition	Equation	Equation in H, Θ, P
Continuity	$U_1 + u_1 = U_2 + u_2$ $U_1 = U_2$ $\therefore u_1 = u_2$	$\Theta_1 - \Theta_2 + A_r P_1 + B_r P_2 = 0$
Constant Leaving Angle	$\frac{V_r - (V_2 + v_2)}{U_2 + u_2} = \tan\beta_2$ $= \text{const.}$	$H_1 = \Theta_1 + \alpha_r P_1 + \beta_r P_2$
Blade Loss Specification	$(\Delta p_0)_{rel} = \rho(U_1 + u_1)^2 P(\tan\beta_1)$	$H_2 = \Theta_2 + \gamma_r P_2$

The first two equations of Table B-I may be written as:

$$\Theta_1 - \Theta_2 + A_r \mathcal{P}_1 + B_r \mathcal{P}_2 = 0 \tag{11}$$

$$\Theta_1 + \alpha_r \mathcal{P}_1 + \beta_r \mathcal{P}_2 = H_1 \tag{12}$$

The complementary equations to these two from the operation of Eqn. 10 are:

$$\mathcal{P}_1 + \mathcal{P}_2 - A_r \Theta_1 - B_r \Theta_2 = 0 \tag{13}$$

$$\mathcal{P}_1 - \alpha_r \Theta_1 + \beta_r \Theta_2 = H_1^* \tag{14}$$

Except for a phase shift (important only if a specific streamline is desired), $H(-\infty, y) = H_1(0-, y)$ is a given function. Also known are the constants A_r, B_r, α_r, β_r, and γ_r. Equations 11 through 14 determine $\mathcal{P}_1$, $\mathcal{P}_2$, Θ_1 and Θ_2. The H_2 can be found from the third matching condition,

$$H_2 = \Theta_2 + \gamma_r \mathcal{P}_2 \tag{15}$$

and the solution is complete.

B2 Theory of Seidel

For a flow field prescribed as for the theory of Rannie and Marble, Seidel has chosen to relax the assumption of constant leaving angle. Experimental evidence of the invalidity of this assumption is shown in Figure 14.

Making use of the Kutta condition, Seidel determines the incremental forces on a single blade in the flow field due to perturbation velocity components normal and parallel to the mean relative

velocity. In this calculation, the Rannie-Marble analysis is used as a first approximation to obtain perturbation components u_1, u_2, v_1, v_2 which are then resolved into components parallel and perpendicular to w_o. The net y-component of "blade force per chord" (non-dimensional) per unit span is then calculated, and this quantity multiplied by chord/pitch ratio to obtain the "force per pitch" per unit span. The influence of blade row effectiveness is introduced as a lattice coefficient which is a function of chord/pitch ratio, stagger and camber.

The three boundary conditions for the Seidel analysis are listed in Table B-II where the blade force specification has replaced the constant leaving angle assumption of Rannie and Marble. Reference 3 includes a detailed treatment of the equivalence of the expressions in u, v, p and those in H, Θ, P. The constant ζ values are fixed by the mean flow, and the values of H, Θ, and P are computed in a manner analogous to that of Rannie and Marble.

TABLE B-II

Boundary Conditions for Seidel

Match Condition	Equation	Equation in H, Θ, P
Continuity	$u_1 = u_2$	$\zeta_1(H_2 - P_2) - \zeta_2 \Theta_2 = \zeta_3(H_1 - P_1) - \zeta_4 \Theta_1$
Relative Bernoulli Equation	$\frac{p_1}{\rho} + (V_1 - \Omega r)V_1 = \frac{p_2}{\rho} + (V_2 - \Omega r)V_2 + \frac{\bar{U} u_1 C_D}{\cos^2 \beta_m} - \frac{C_D'}{2}(\Theta_1 + \Omega r u_1)\frac{1}{\cos^2 \beta_m}$	$\zeta_{17}\Theta_1 - \zeta_{18}\Theta_2 + \zeta_{18} P_1 - P_2 = \zeta_{19} H_1$
Blade Force Specification	$\frac{-\Delta F_Y}{\rho S} = \bar{U}(v_1 - v_2) + u(V_1 - V_2)$	$\zeta_{20}\Theta_1 - \Theta_2 - \zeta_9 P_1 = -\frac{\Delta F_Y}{\rho S} - \zeta_9 H_1$

B3 Calculations

The calculation time required for each theoretical curve of Figure 9 can be appreciated when it is remembered that a system of four simultaneous equations must be solved for each of 51 input points (H_1/U^2). To reduce the manual computation time for both methods of analysis, it was convenient to program the numerical work for the IBM 704 Electronic Data Processing Machine at the M.I.T. Computation Center. Flow diagrams and further details of the programming and computation procedure are found in Reference 3.

APPENDIX C

Influence of Turbulence on Pressure Measurements

In the measurement of flow immediately behind the distortion screen or the rotor, it is probable that pressure readings are in error due to the high turbulence level in these regions. The pressure tap in turbulent flow no longer measures only the pressure of the stagnant air just inside the opening, but includes a non-zero, time-average increment of pressure resulting from the turbulence velocity component normal to the plane of the opening.

Reference 7 indicates that the turbulence-induced pressure components for static and stagnation measurements are identical for isotropic turbulence. Thus, for velocity calculations with isotropic turbulence, the indicated pressures may be used without correction, since the turbulence components are self-cancelling.

There is, however, experimental evidence that the turbulence immediately behind a grid is anisotropic. In Figure 5 and Figure 6 of Reference 8, for a flow velocity comparable to that of the present experiments, the longitudinal component of turbulence is shown to be predominant, even at some distance from the turbulence producing grid.

In the experiments for this thesis, pressure measurements in the region immediately downstream of a distortion screen demonstrate a measure of scatter (not observed in the region between screens) which may be attributed to turbulence. Based on the evidence of Reference 8, this turbulence may be assumed anisotropic, in which case the three-hole probe measures a turbulence-induced increment of stagnation pressure which

is larger than the turbulence-induced component of static pressure.

Thus in mean-velocity calculations for low speed flow (that is, where the flow is assumed incompressible and $V \sim \sqrt{p_o - p}$) in regions where anisotropic turbulence is indicated (e.g., immediately downstream of a distortion screen or rotor) a value higher than the true time-mean value would be anticipated.

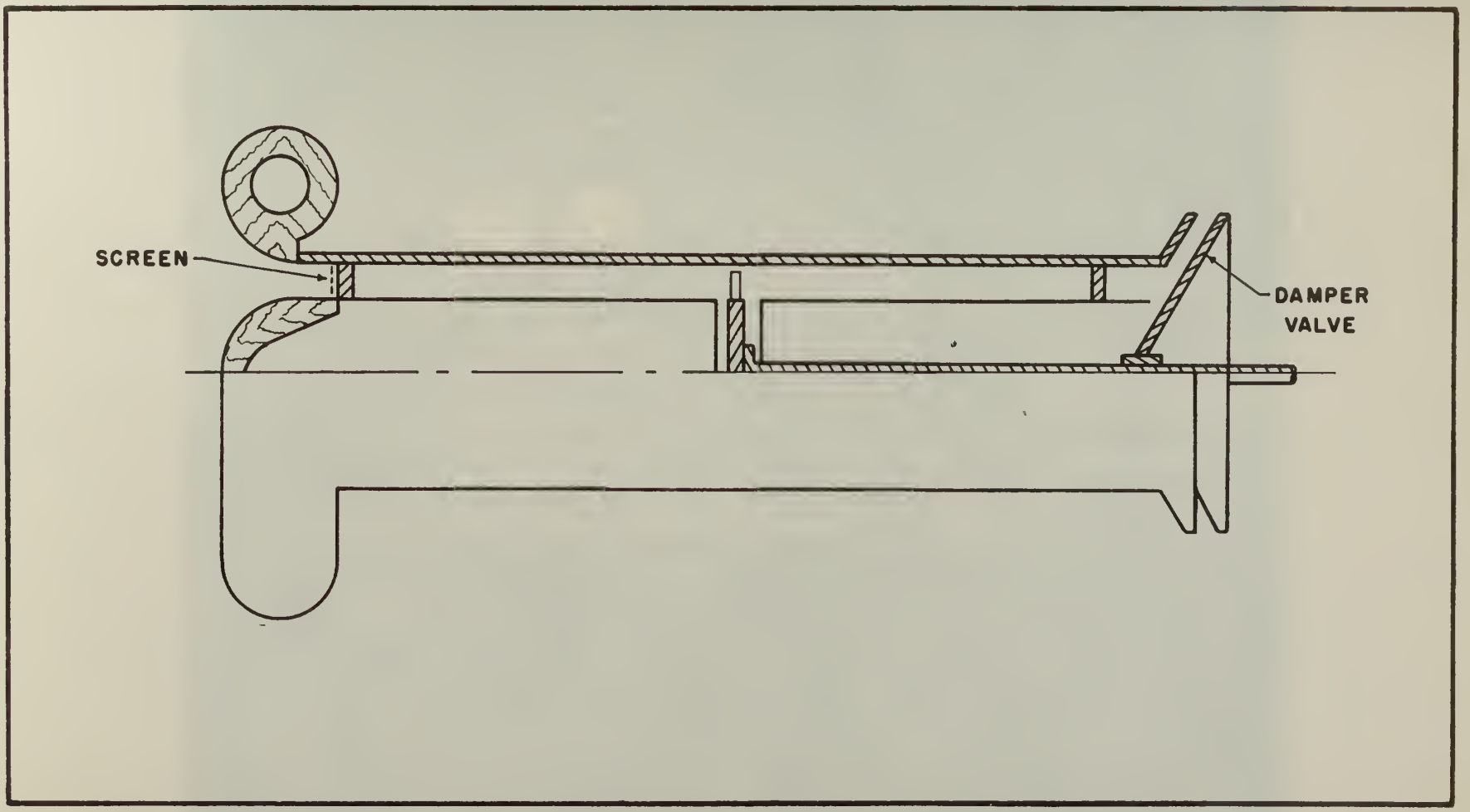

FIG. 1 SECTION VIEW OF COMPRESSOR

FIG. 2 VIEW OF ROTOR (2b/S=0.525) WITH CASING REMOVED

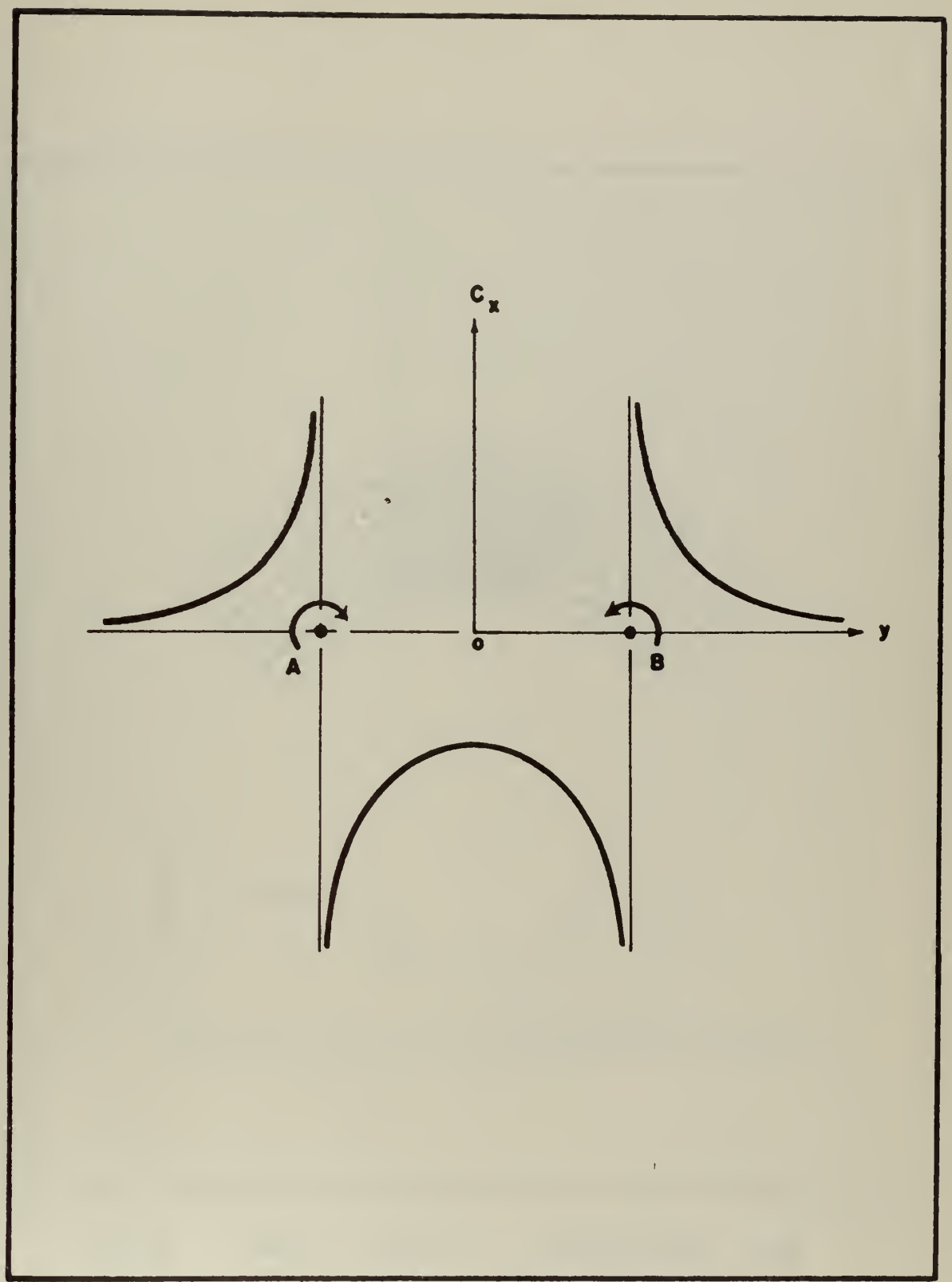

FIG. 3 VELOCITY DISTRIBUTION FOR
A PAIR OF
POINT VORTICES A, B

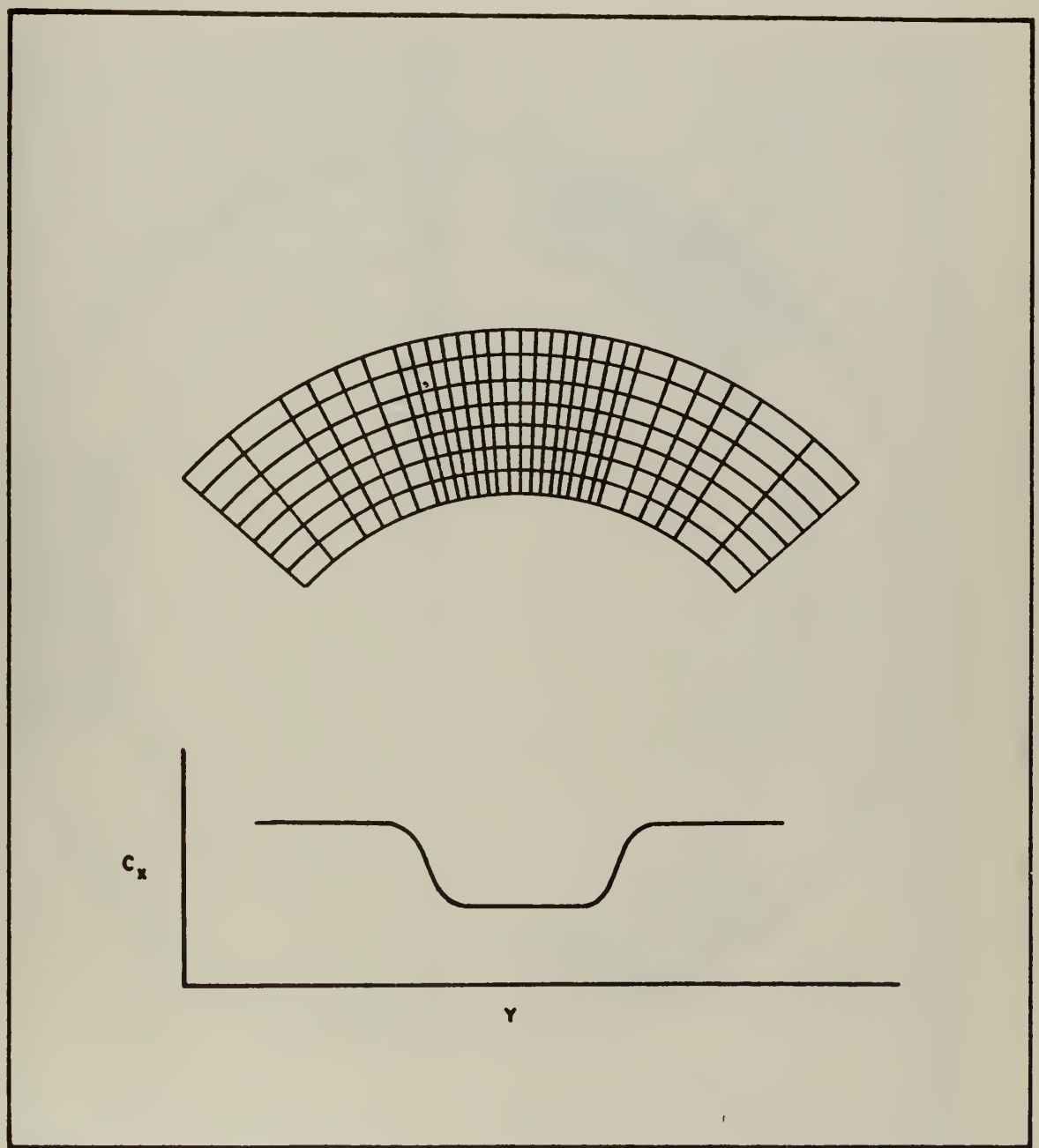

FIG. 4 IDEAL SOLIDITY DISTRIBUTION FOR A SQUARE WAVE PROFILE

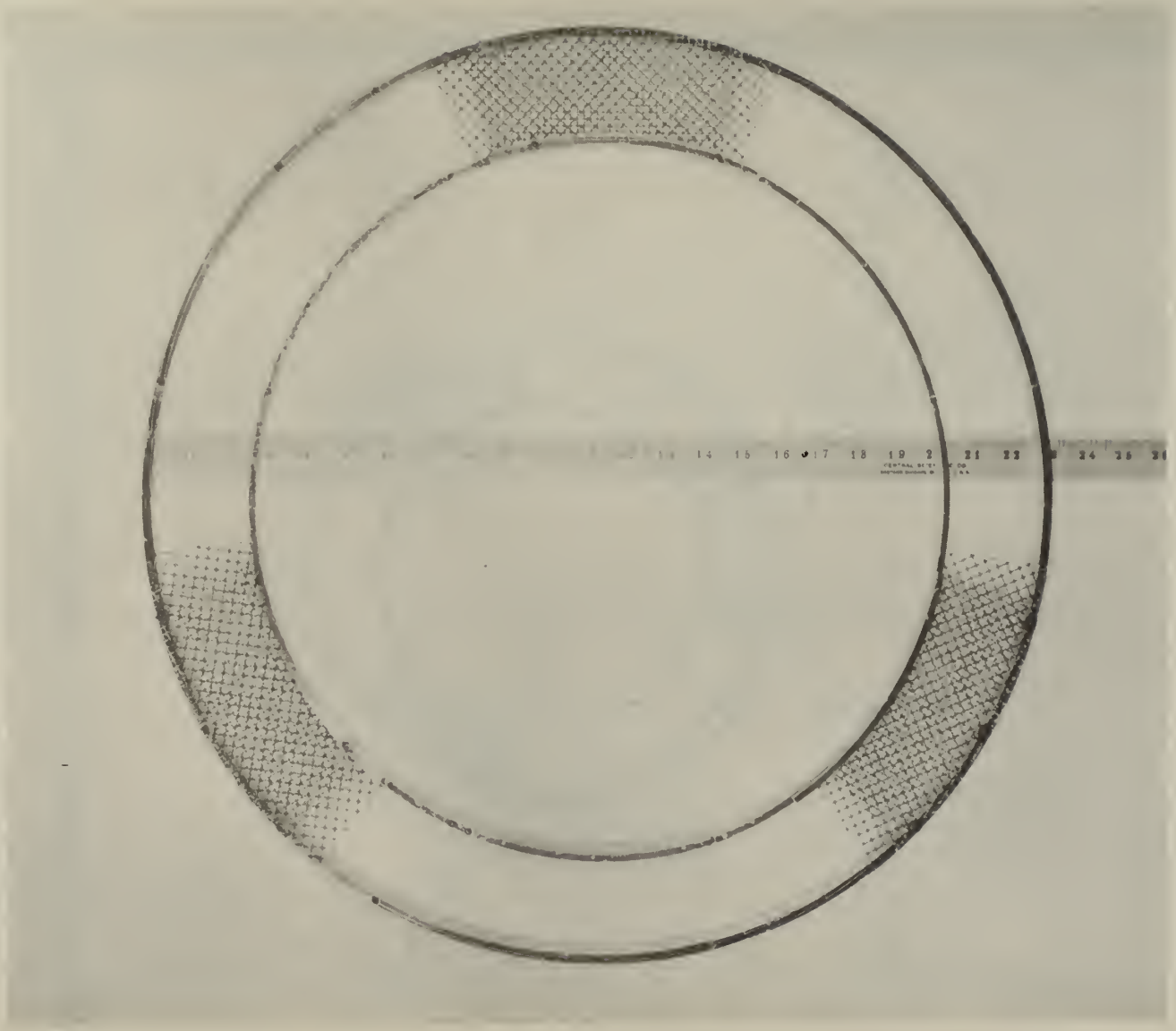

FIG. 5 DISTORTION SCREENS AND FRAME

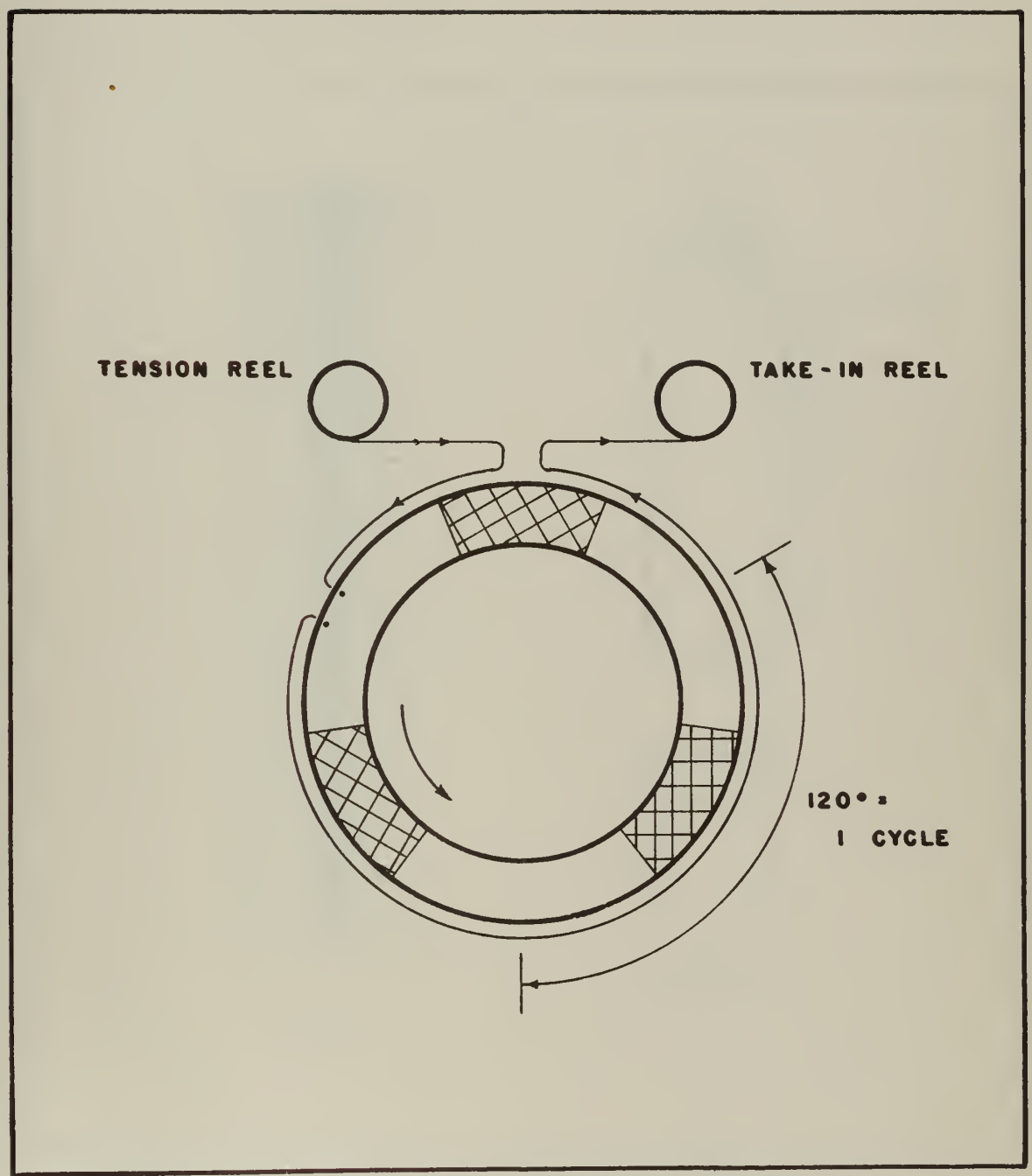

FIG. 6 REEL AND CORD ARRANGEMENT

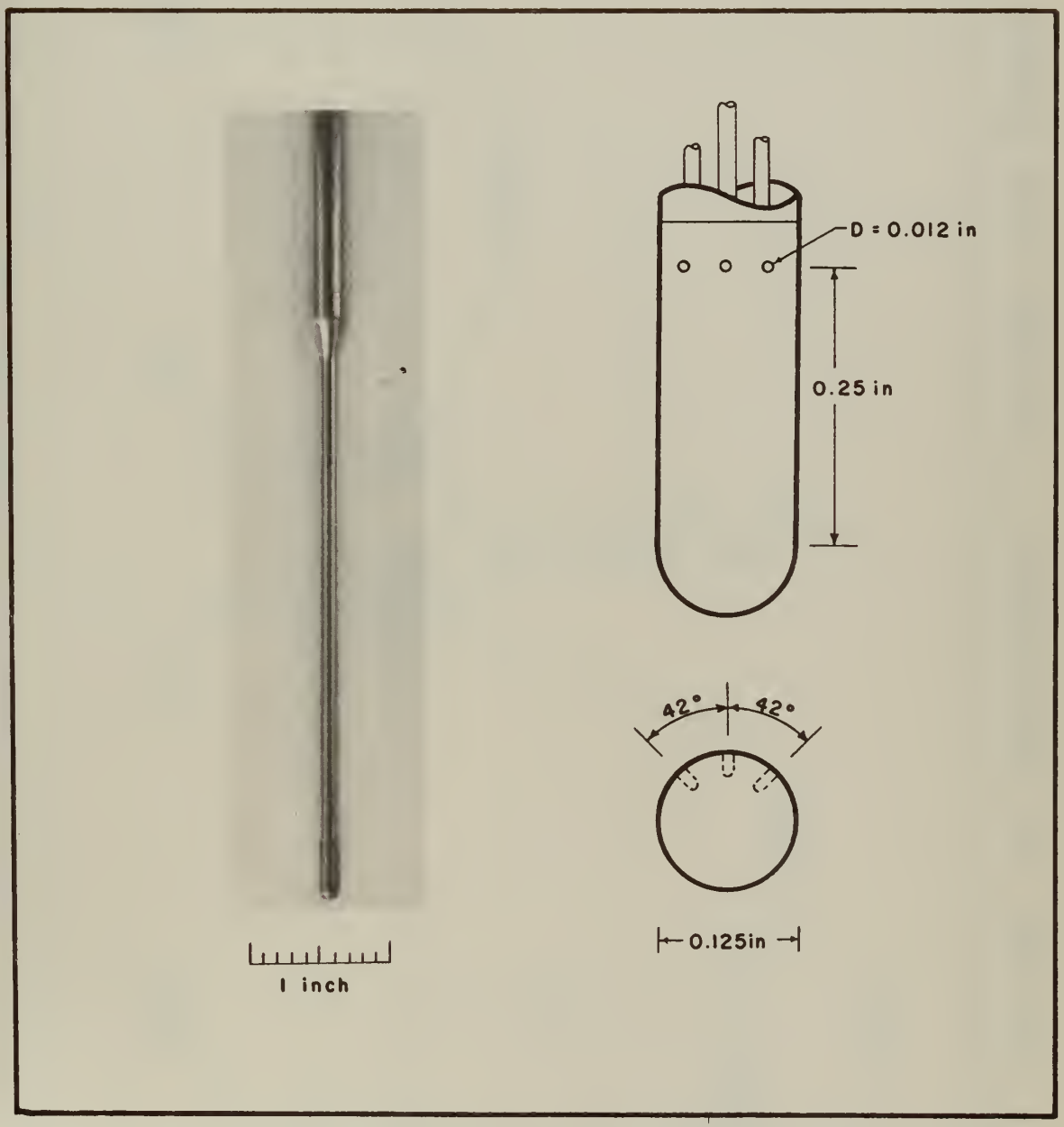

FIG. 7 THREE-HOLE FECHEIMER TUBE AND DETAILS

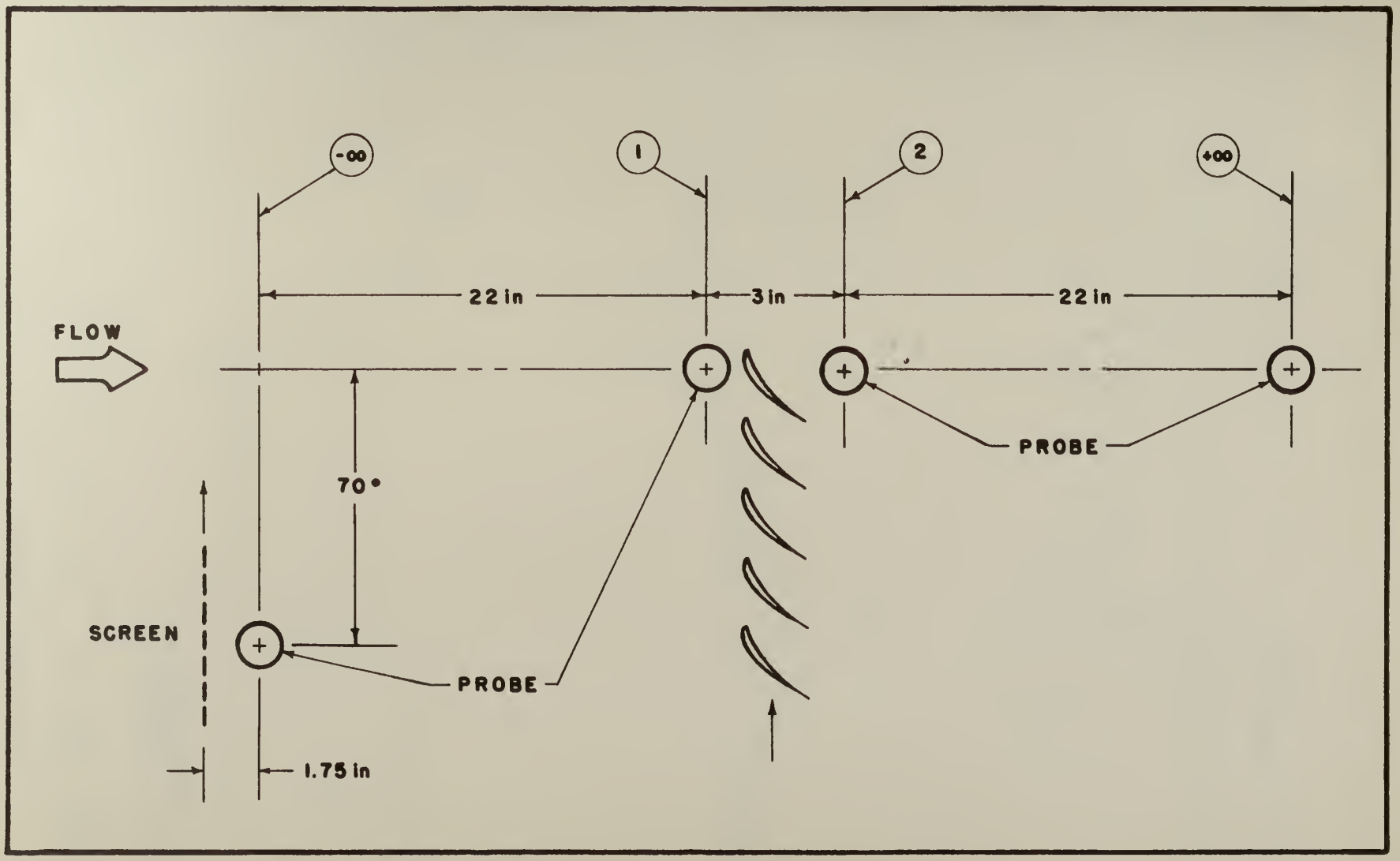

FIG. 8 LOCATION OF MEASUREMENT STATIONS AND SCREEN

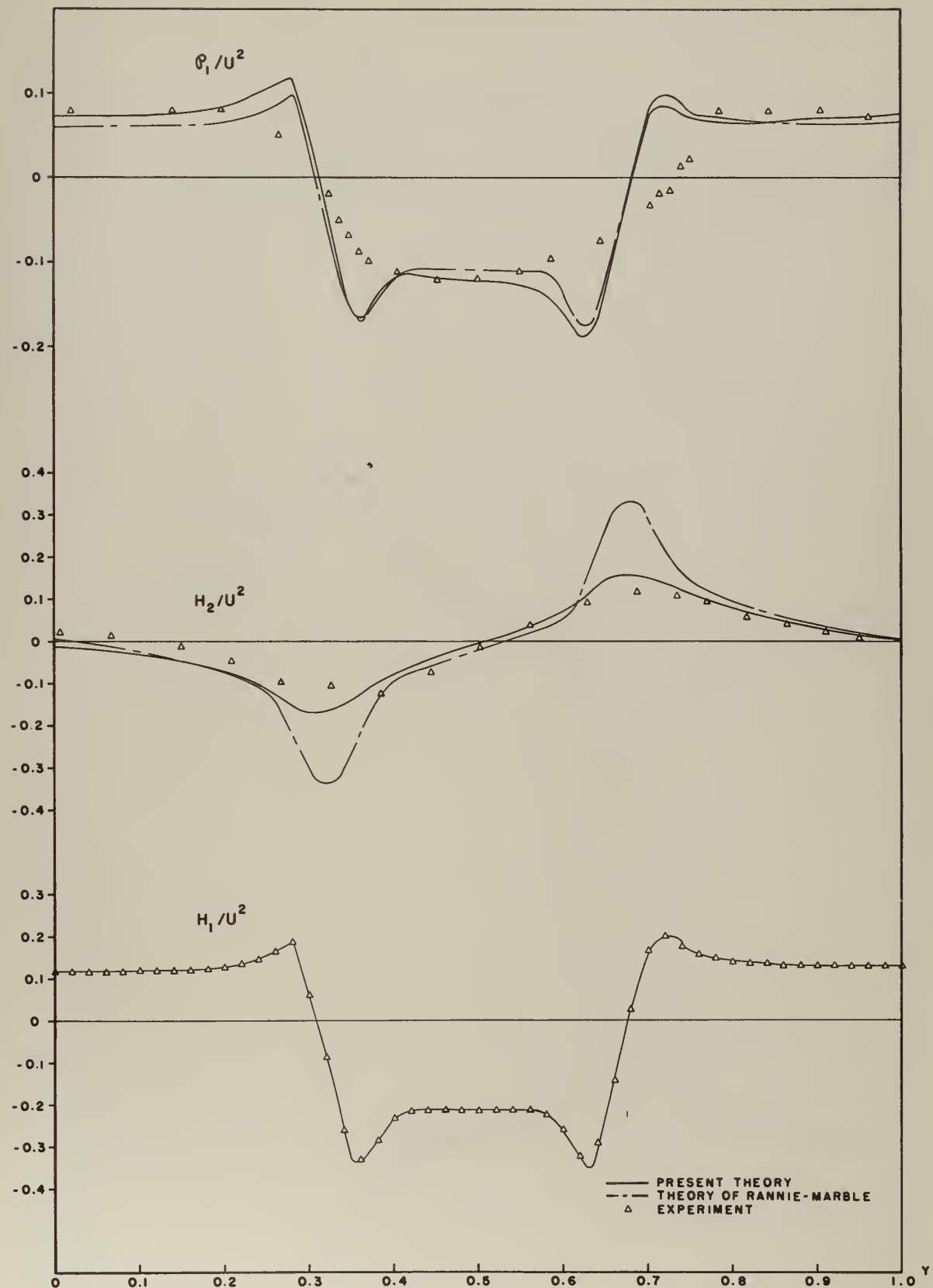

FIG. 9-1 PERTURBATIONS UPSTREAM AND DOWNSTREAM, THEORY AND EXPERIMENT. $2b/S = 1.05$, $U/\Omega r = .562$

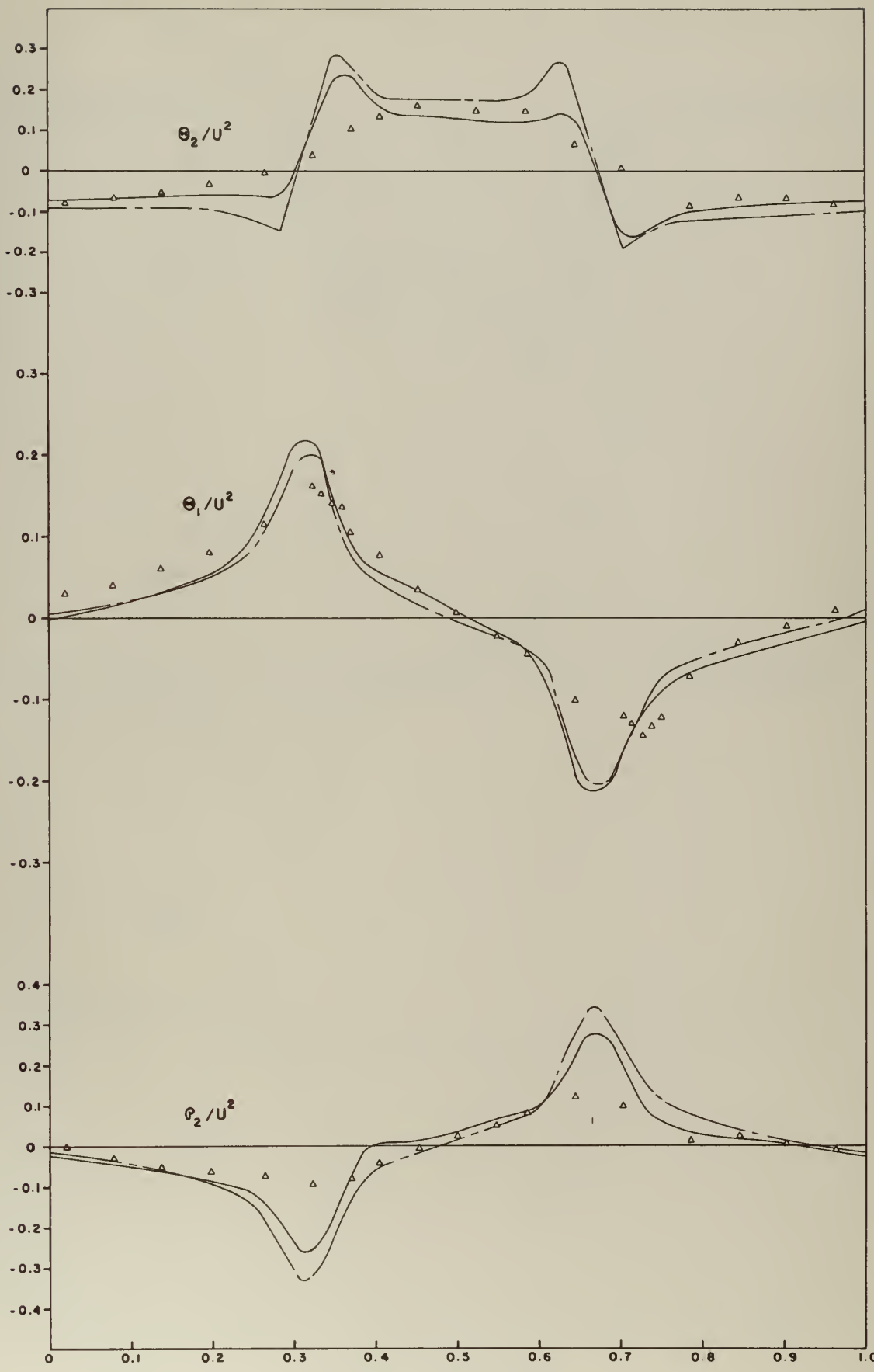

FIG. 9-1 CONTD.

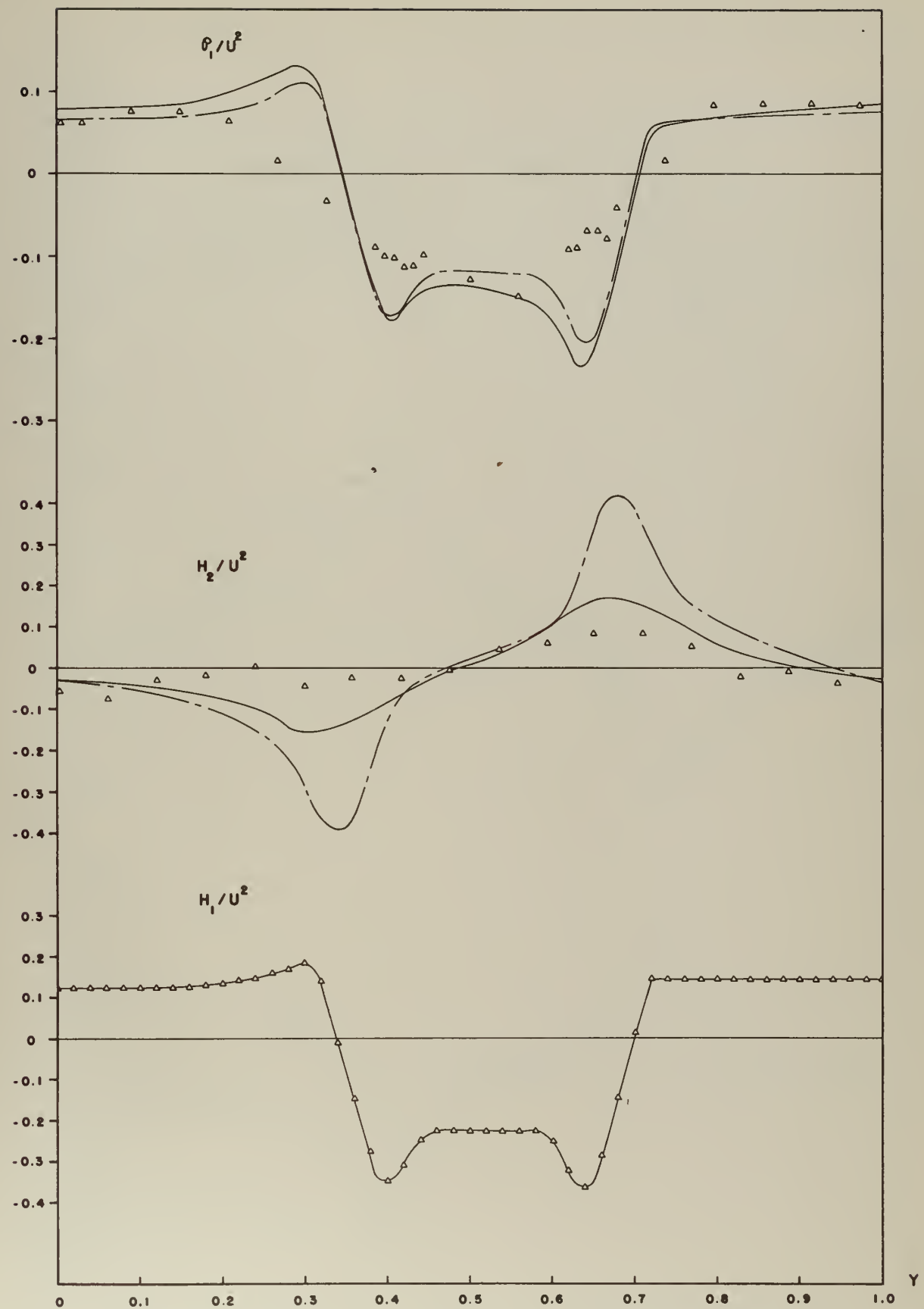

FIG. 9 -2 $2b/S = 1.05$, $U/\Omega r = .460$

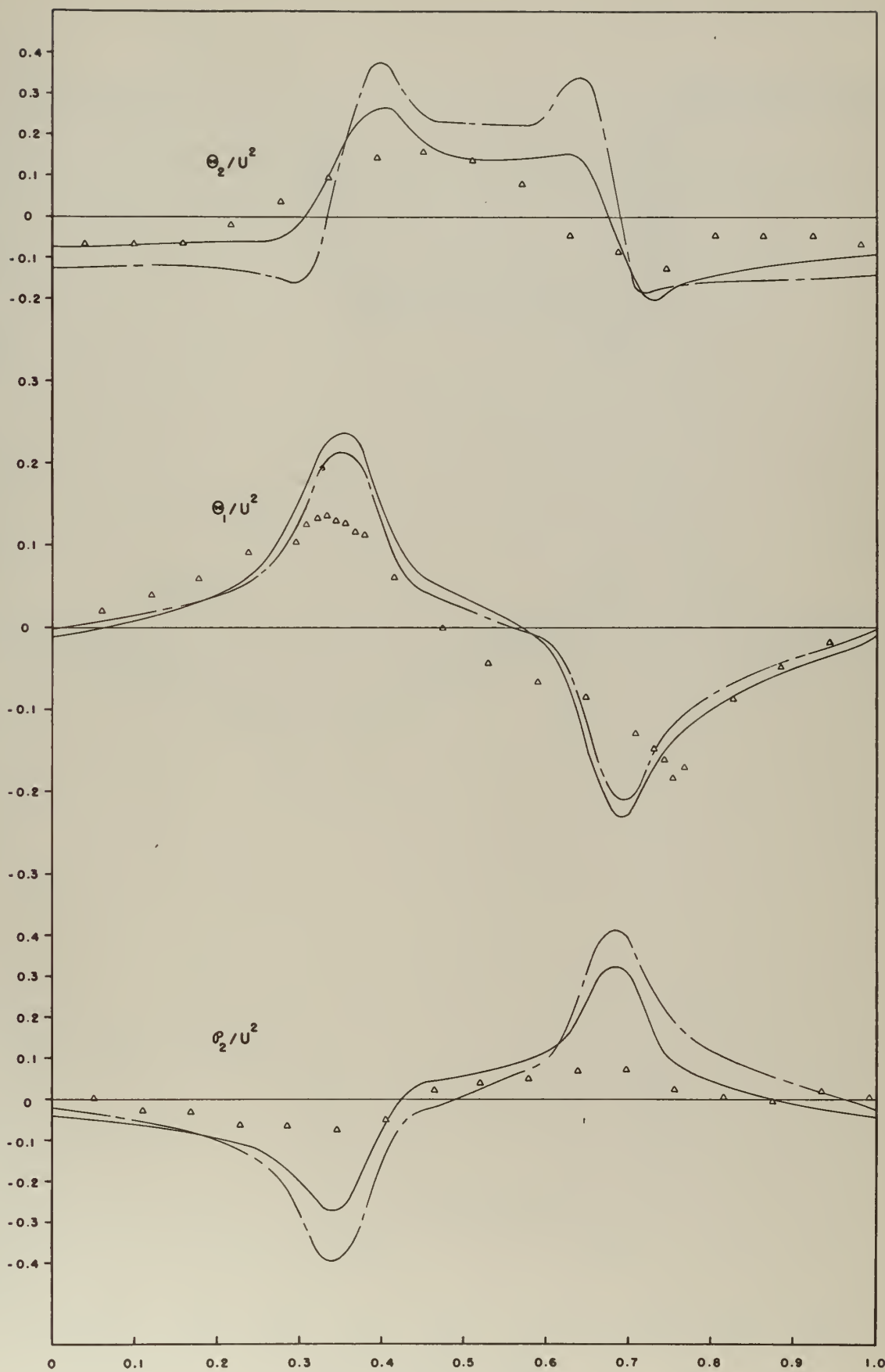
Θ_2/U^2
Θ_1/U^2
ρ_2/U^2
0.4
0.3
0.2
0.1
0
-0.1
-0.2
-0.3
-0.4
0
0.1
0.2
0.3
0.4
0.5
0.6
0.7
0.8
0.9
1.0
Y

FIG. 9-2 CONTD.

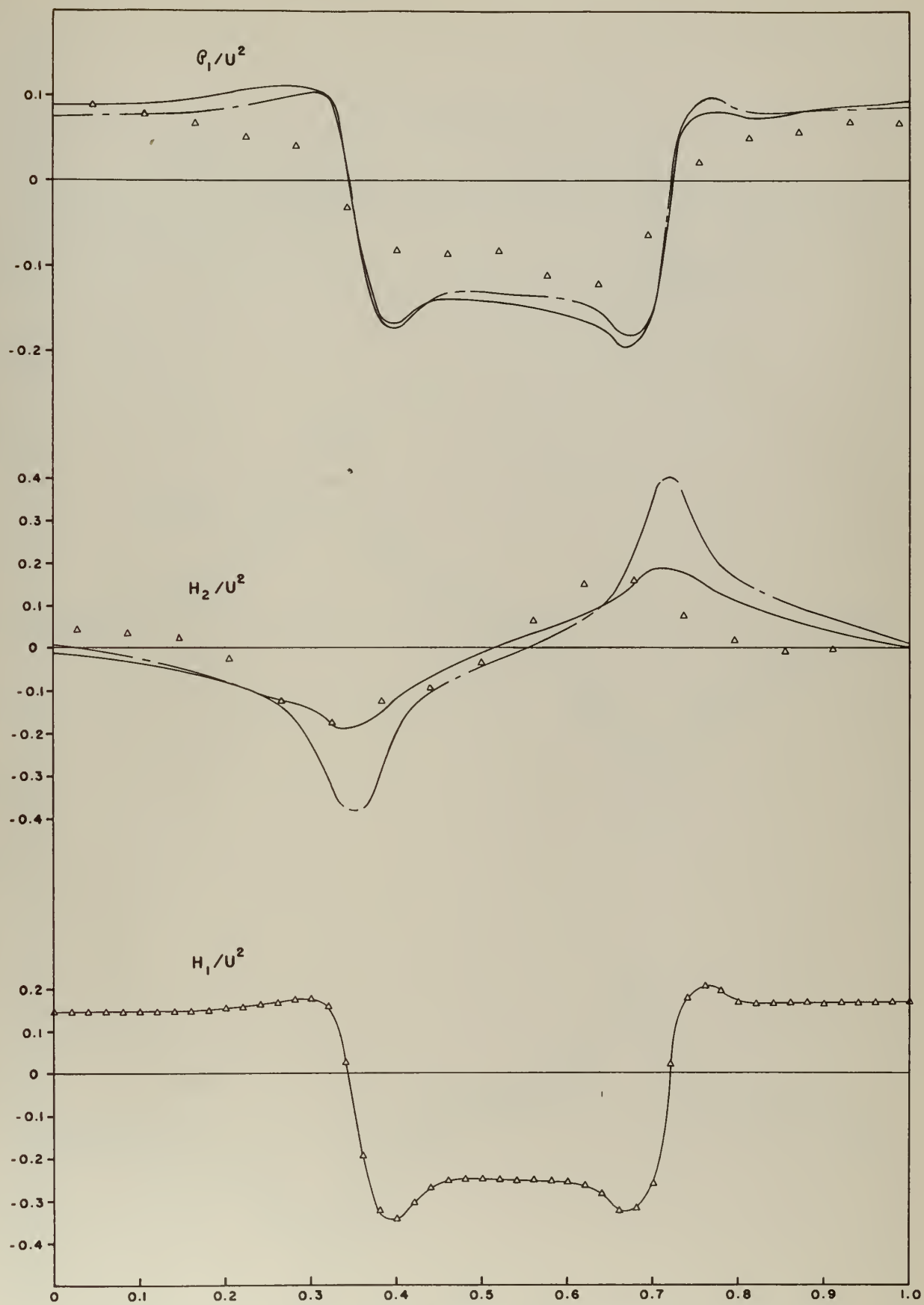

FIG. 9-3 $2b/S = .525$, $U/\Omega r = .514$

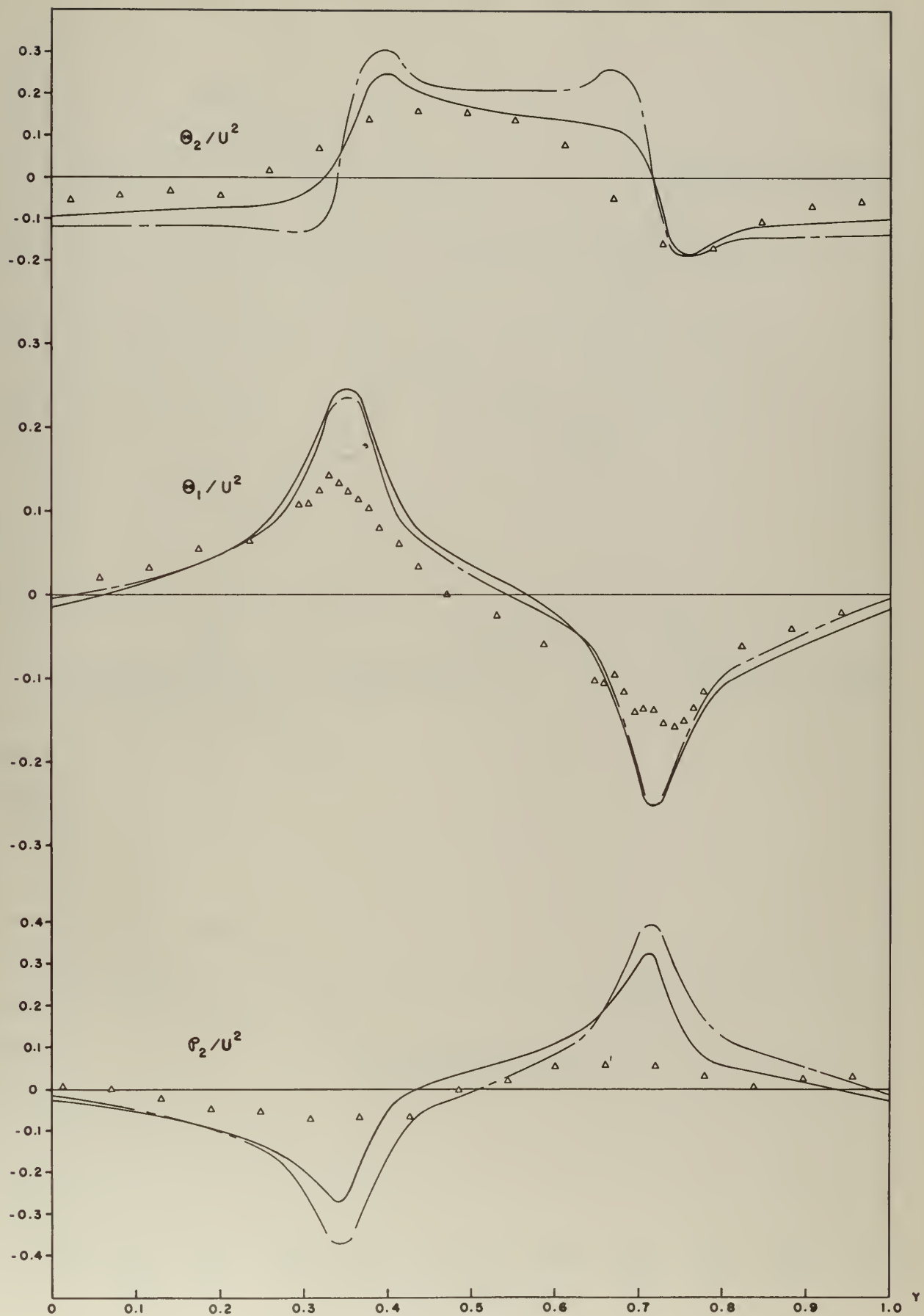

FIG. 9-3 CONTD.

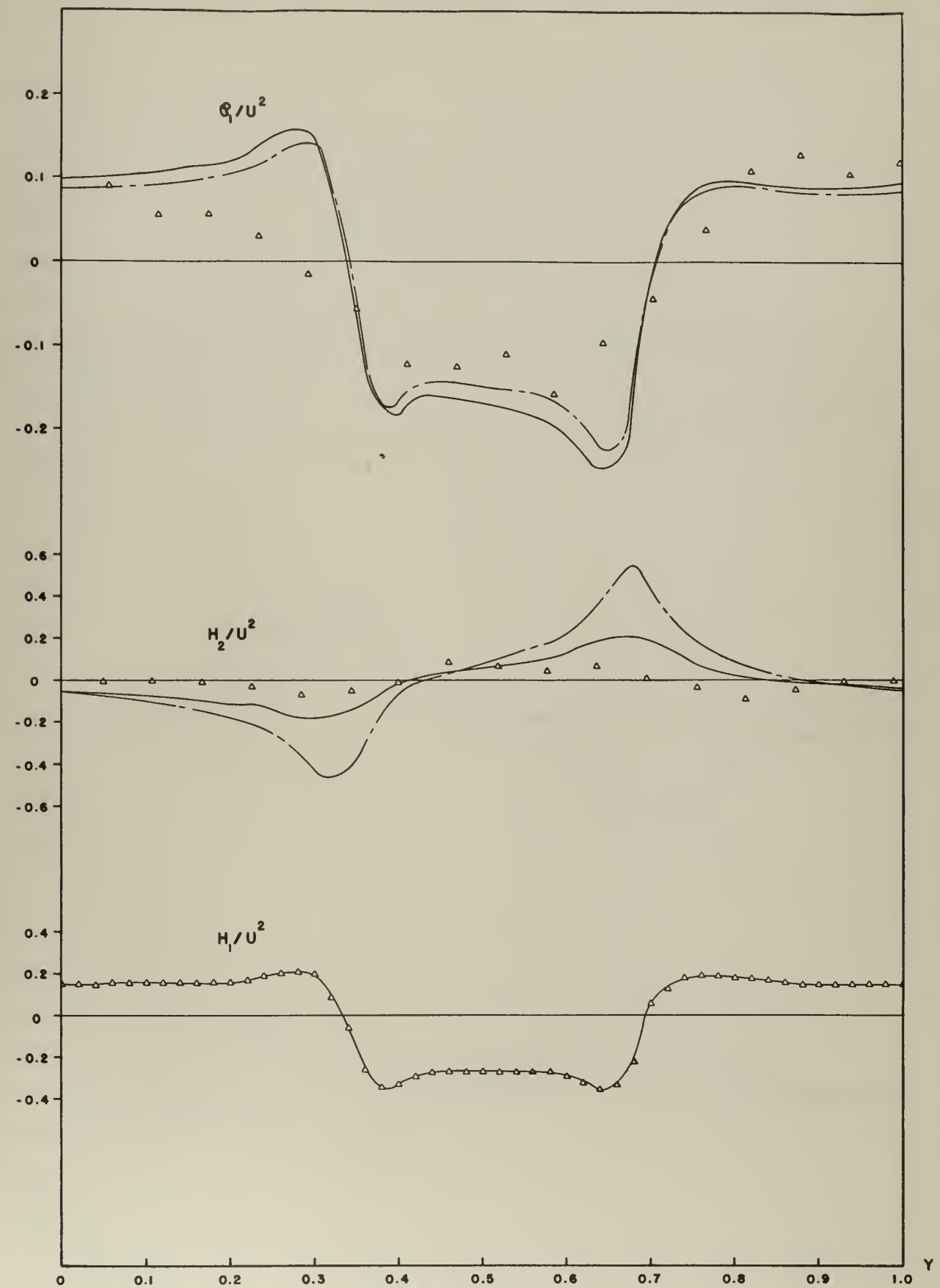

FIG. 9-4 $2b/S = .525,\ U/\Omega r = .391$

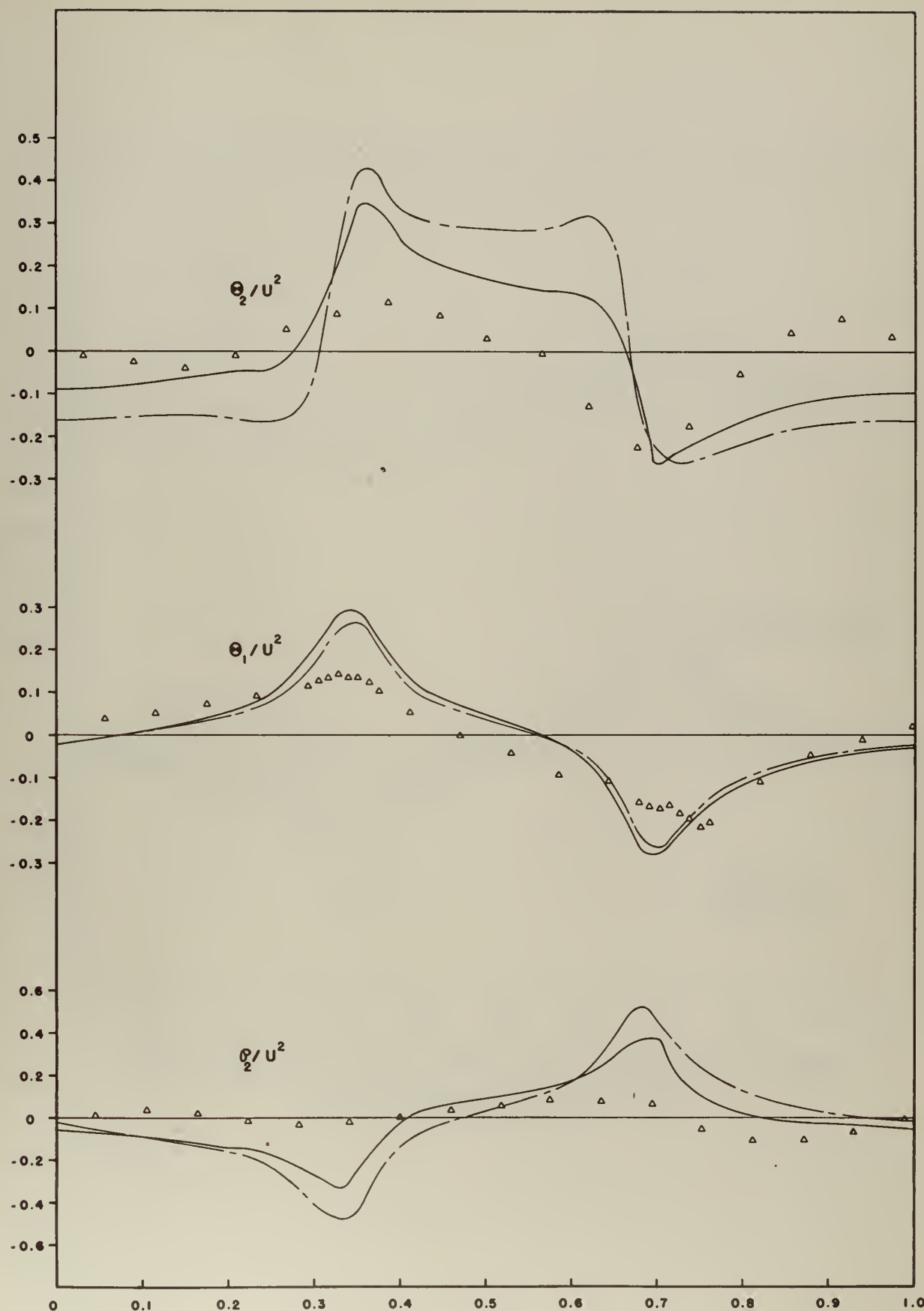
0.5
0.4
0.3
0.2
0.1
0
-0.1
-0.2
-0.3
Θ_2/U^2
0.3
0.2
0.1
0
-0.1
-0.2
-0.3
Θ_1/U^2
0.6
0.4
0.2
0
-0.2
-0.4
-0.6
Φ_2/U^2
0
0.1
0.2
0.3
0.4
0.5
0.6
0.7
0.8
0.9
1.0
Y

FIG. 9-4 CONTD.

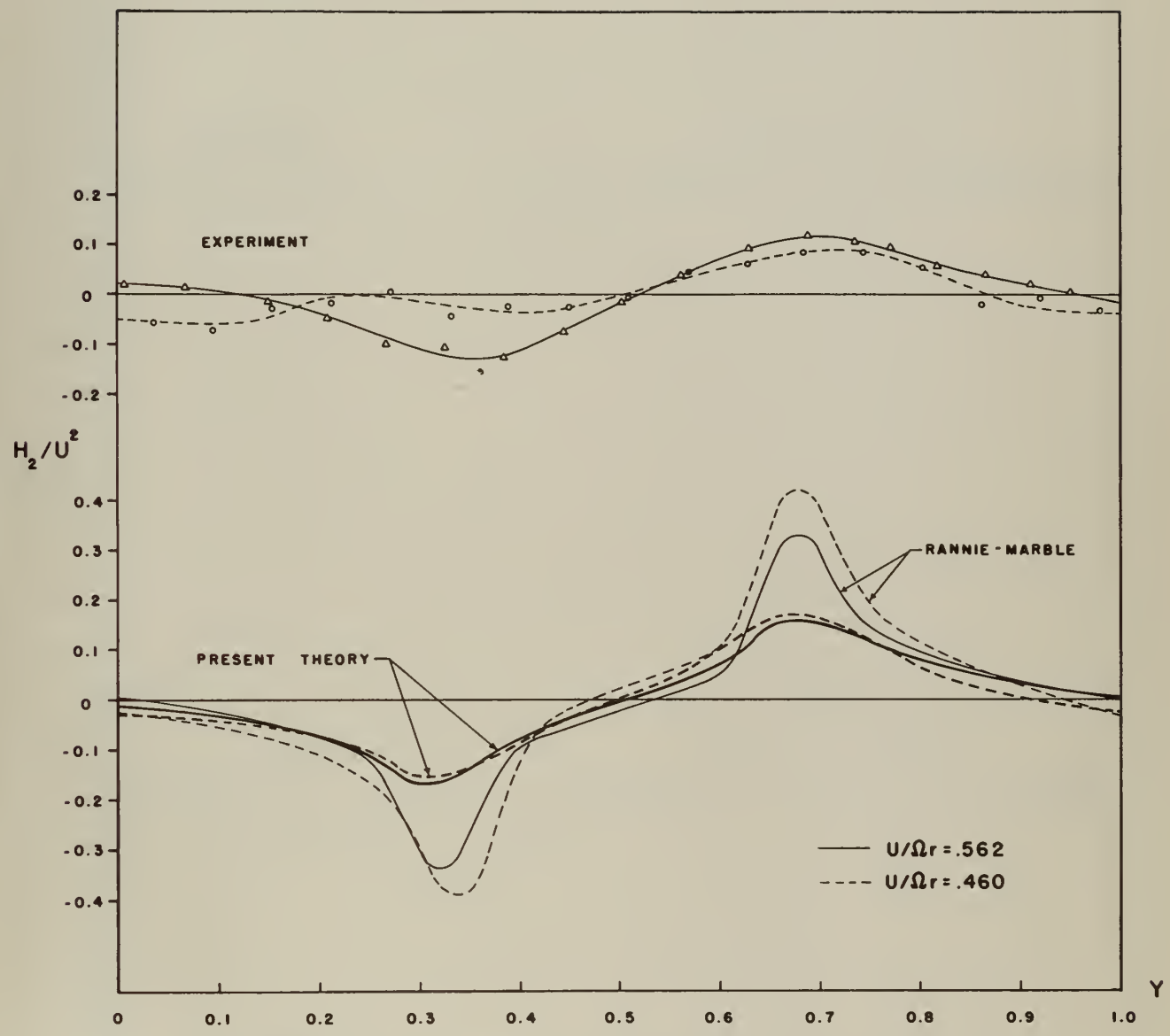

FIG. 10 EFFECT OF FLOW RATE ON ATTENUATION, THEORY AND EXPERIMENT. 2b/S = 1.05

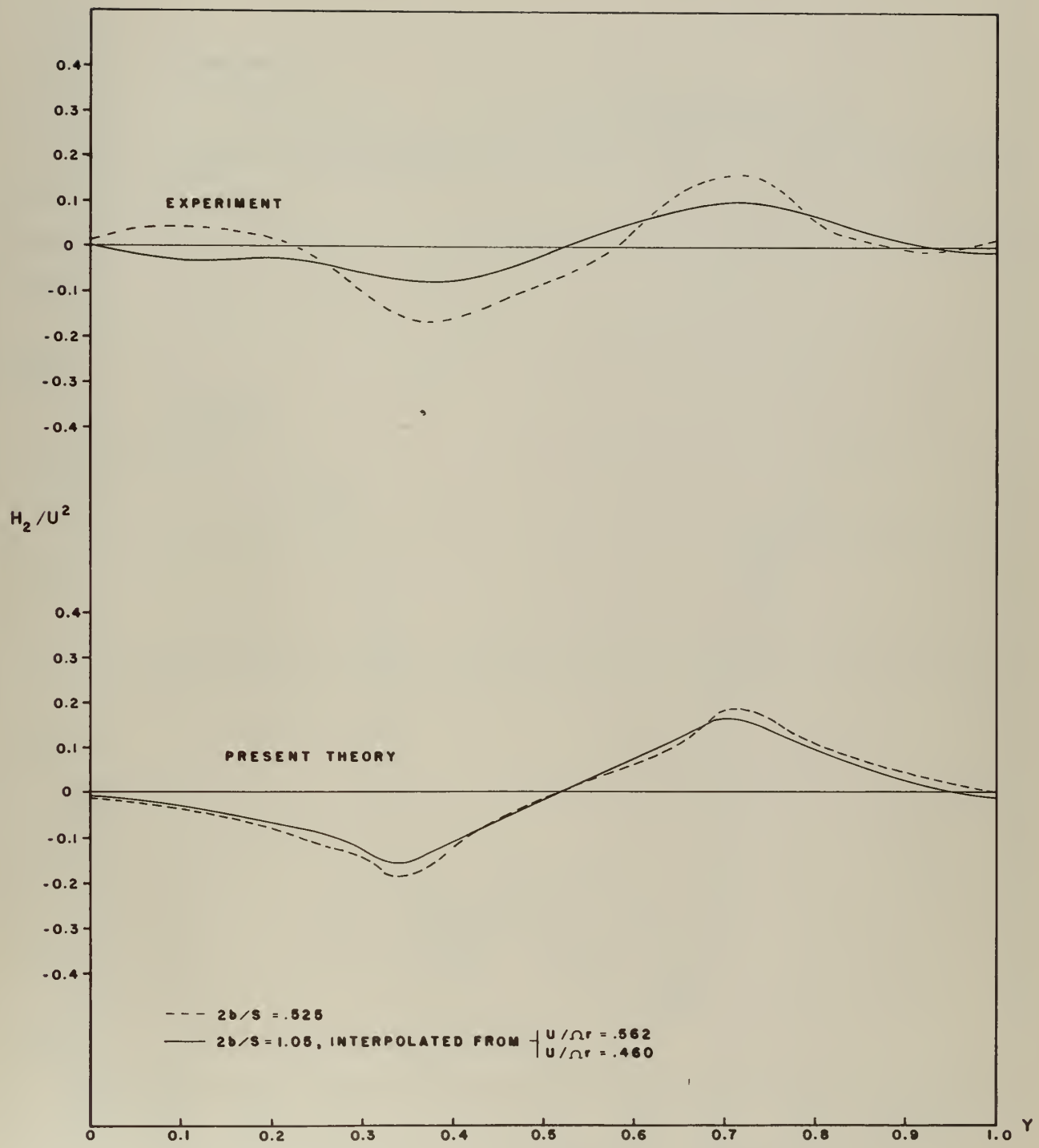

FIG. 11 EFFECT OF SOLIDITY ON ATTENUATION, THEORY AND EXPERIMENT, $U/\Omega r = .514$

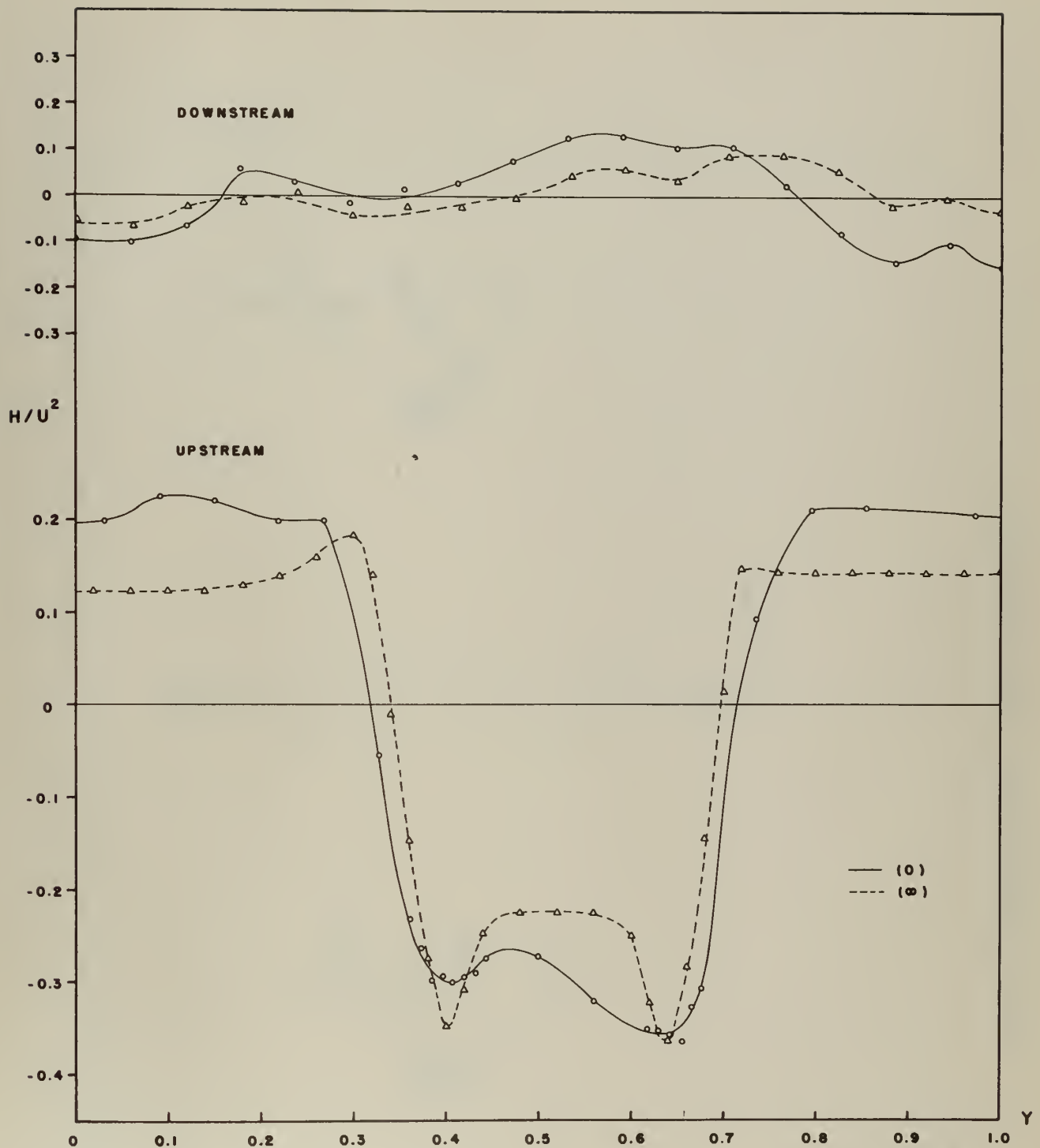

FIG. 12 COMPARISON OF EXPERIMENTAL $H_{-\infty}/U^2$ AND H_{-0}/U^2 (UPSTREAM); H_{+0}/U^2 AND $H_{+\infty}/U^2$ (DOWNSTREAM)

$2b/S = 1.05$, $U/\Omega r = .460$

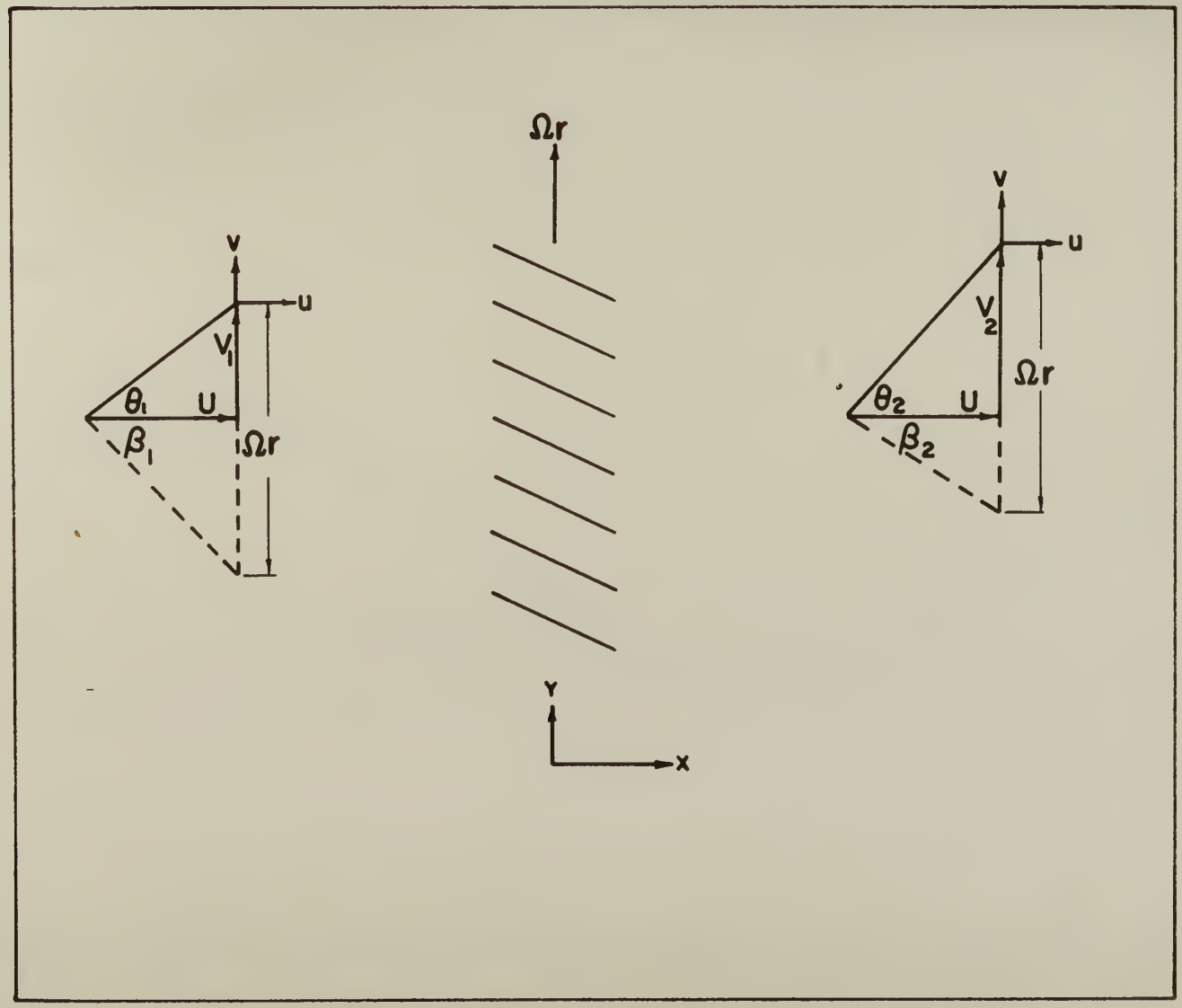

FIG.13 COORDINATES AND NOTATION

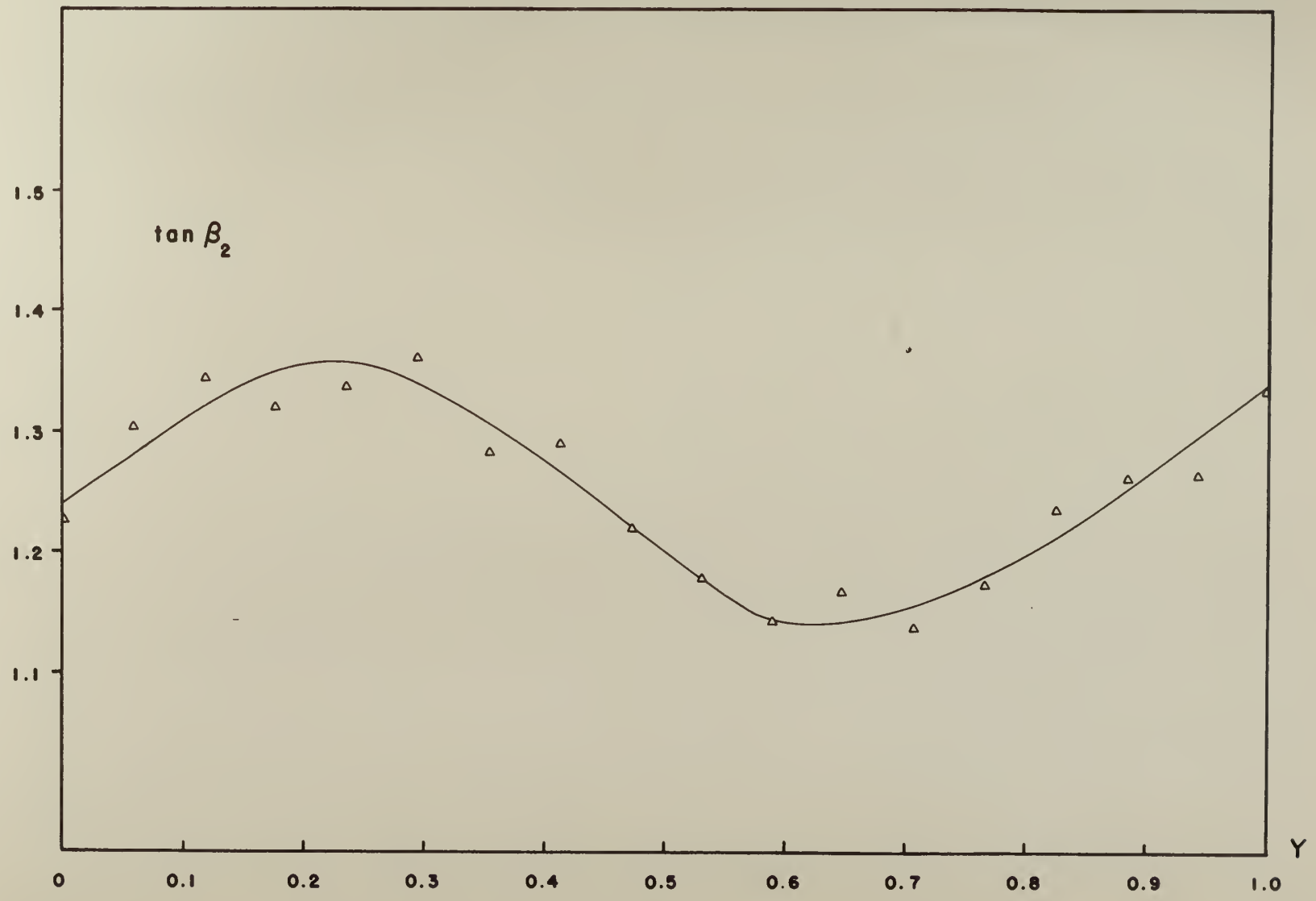

FIG.14 VARIATION IN $\tan \beta_2$ WITH Y ($2b/S = 1.05, U/\Omega r = .460$)